



DEGREE PROJECT IN ENGINEERING PHYSICS,
SECOND CYCLE, 30 CREDITS
STOCKHOLM, SWEDEN 2020

Development and 3D Printing of Intrinsically Stretchable Materials for Microsupercapacitors

ALEXANDER ENGMAN

IA249X DEGREE PROJECT IN ENGINEERING PHYSICS

Development and 3D Printing of Intrinsically Stretchable Materials for Microsupercapacitors

Author:

ENGMAN, Alexander

Examiner:

LI, Jiantong

Supervisor:

MISHUKOVA, Viktoriia

Co-supervisor:

CHENG, Shi

KTH Royal Institute of Technology

School of Electrical Engineering and Computer Science

SE-100 44 Stockholm

Abstract

The purpose of this thesis is to develop a simple Direct Ink Writing (DIW) method for fabricating intrinsically stretchable microsupercapacitors as effective on-chip energy storage devices for the emerging stretchable electronics. Using the printing method for fabricating intrinsically stretchable electronic components remains a novel approach. In this thesis, interdigitated structures of intrinsically stretchable electrodes were printed on a stretchable thermoplastic polyurethane (TPU) substrate using a formulated ink based on Poly(3,4-ethylenedioxythiophene):Polystyrene Sulfonate. Formulated electrolytes based on Poly(4-styrene Sulfonic Acid) and Phosphoric Acid were applied to the electrodes to complete the fabrication of microsupercapacitors. Cyclic Voltammetry (CV), Galvanostatic Charge-Discharge (GCD) and Electrochemical Impedance Spectroscopy (EIS) were used to characterize the performance of the devices. The stretchability of the electrodes was also measured. Results from CV-measurements revealed a maximum capacitance of $740 \mu\text{F cm}^{-2}$ at a scan rate of 5 mV s^{-1} . GCD-measurements showed a capacitance of $952 \mu\text{F cm}^{-2}$ for the same device and an equivalent series resistance of approximately $7 \text{ k}\Omega$. The printed electrodes exhibited a stretchability of 80%. The results show the feasibility of fabricating intrinsically stretchable energy storage devices using commercially available materials and a simple 3D printing technique. This method could be used as a high-throughput and low-cost method for stretchable electronics applications.

Keywords

Stretchable electronics, Printed electronics, 3D printing, Direct Ink Writing, Additive manufacturing, Printed supercapacitor

Sammanfattning

Syftet med detta arbete är att utveckla en simpel Direct Ink Writing (DIW) metod för framställning av intrinsiskt sträckbara mikrosuperkondensatorer som effektiva on-chip energilagringsenheter i kommande sträckbar elektronik. Användandet av DIW för att tillverka intrinsiskt sträckbara elektroniska komponenter är ett nytt tillvägagångssätt. I detta arbete trycktes interdigiterade strukturer av intrinsiskt sträckbara elektroder på ett sträckbart termoplastiskt polyuretan (TPU) substrat genom att använda ett formulerat bläck baserat på Poly(3,4-etylendioxidfen):Polystyren Sulfonat (PEDOT:PSS). Formulerade elektrolyter baserade på Poly(4-styrensulfonsyra) och Fosforsyra applicerades på elektroderna för att färdigställa tillverkningen av mikrosuperkondensatorer. Cyklisk Voltammetri (CV), Galvanostatisk uppladdning-urladdning (eng. GCD) och Elektrokemisk Impedansspektroskopi (EIS) användes för att karakterisera enheternas prestanda. Bläckets sträckbarhet uppmättes också. Resultaten från CV-mätningar visade att den maximala kapacitansen var $742 \mu\text{F cm}^{-2}$ vid skanningsfrekvensen 5 mV s^{-1} . Kapacitansen från GCD-mätningar var $952 \mu\text{F cm}^{-2}$ för samma enhet och den ekvivalenta serieresistansen var cirka $7 \text{ k}\Omega$. Sträckbarheten som de tryckta elektroderna uppvisade var 80%. Resultaten påvisar möjligheten att kunna framställa intrinsiskt sträckbara energilagringsenheter genom att använda kommersiellt tillgängliga material och en simpel metod för friformsframställning. Denna metod skulle kunna användas för att framställa sträckbara elektroniska komponenter till låg kostnad och med hög produktionstakt.

Nyckelord

Sträckbar elektronik, Tryckt elektronik, Friformsframställning, Direct Ink Writing, Additiv tillverkning, Tryckt superkondensator

Acknowledgements

I would like to express my sincere gratitude to my examiner and co-supervisor Dr. Jiantong Li and to my main supervisor Viktoriia Mishukova for allowing me to participate in their research. Their involvement in the work has been invaluable in guiding me through the various parts of the thesis project. The constant feedback and close collaboration has allowed me to constantly improve the practical work as well as my own understanding of the subject. I have gained a lot of experience that will be very useful in my future.

I would like to thank Han Xue and Mika-Matti Laurila for their valuable feedback and comments during my various presentations and during discussions. Their insights allowed me to improve my work and many details related to my thesis. My special thanks are also extended to Prof. Matti Mäntysalo and Mr. Milad Mosallaei from Tampere University (TAU) for performing stretchability tests on the developed materials. Their contributions were invaluable in showing the importance and validity of this thesis.

Alexander Engman
Stockholm, June 2020

Table of contents

1	Introduction	1
1.1	Background	1
1.2	Problem	1
1.3	Purpose	2
1.4	Goal	2
1.5	Methodology	3
1.6	Outline	5
2	Theoretical background	7
2.1	Printing technology in electronics	7
2.2	State-of-the-art printing techniques	10
2.3	Printed electronics in energy storage	12
2.4	Stretchable microsupercapacitors	17
2.5	Approaches to stretchable MSCs	20
2.6	Properties of PEDOT:PSS	24
3	Methodology	27
3.1	Research strategies	27
3.2	Methods	27
3.3	Data collection and analysis	31
3.4	Quality assurance	32
4	Experimental	33
4.1	Materials	33
4.2	Procedure	36
4.3	Issues	39
5	Results	43
5.1	Electrochemical characterization	43
5.2	Materials characterization	56
6	Conclusions	58
6.1	Outlook	58
	References	64
	Appendix	65

List of Figures

1-1	Schematic description of the quantitative research process. Adapted from [5].	3
1-2	Simplified description of different research approaches.	5
2-1	Evolution of printed electronics.	8
2-2	Stretchable luminescent screen. Reprinted with permission from [9]. Copyright (2019) American Chemical Society.	9
2-3	The main methods of incorporating electronics on human skin. Reprinted with permission from [10]. Copyright (2017) American Chemical Society.	9
2-4	Schematic description of three common AM methods.	11
2-5	Ragone plot displaying the trade-off between power density and energy density. Adapted from [12, 15].	12
2-6	Top figure: Parts of a charged EDLC: (a) current collector, (b) electrode, (c) electric double layer, (d) electrolyte, (e) separator. Bottom figure: Equivalent electrical circuit for an EDLC.	14
2-7	Detailed description of the basic mechanism of an EDLC. Adapted from [15].	15
2-8	Common designs for high-performance energy storage devices.	16
2-9	Basic idea behind a structurally stretchable electrode.	20
2-10	Example of a structurally stretchable electrode. Courtesy of [35].	21
2-11	Basic function of an intrinsically stretchable electrode.	22
2-12	Specific properties of PEDOT:PSS.	24
2-13	Modeling of PEDOT:PSS as a 2-phase material. Adapted from [41].	25
2-14	Morphology change when adding STEC enhancers to PEDOT:PSS. Figure courtesy [31, Fig. 1].	26
3-1	Typical appearance of a CV plot for an EDLC.	28
3-2	Typical appearance of a GCD plot for an EDLC.	29
3-3	Schematic plots from EIS-measurements of a supercapacitor. .	30
3-4	Randles equivalent electrical circuit.	31
4-1	Main parts of the Felix Pro2 3D printer. Courtesy of [43].	33
4-2	Viscotec Vipro-HEAD3 used for 3D printing.	35
4-3	Experimental process of fabrication and measurement.	38

4-4	Common issues associated with the 3D printing process.	40
4-5	U-shape patterns for ink stretchability measurements.	41
4-6	Test setup used for stretchability tests of the formulated ink. The measurements were performed at Tampere University (TAU). The value of L_0 was 50 mm	42
5-1	CV measurements of 1-layer electrodes with EL1.	44
5-2	CV measurements of 2-layer electrodes with EL1.	45
5-3	CV measurements of 4-layer electrodes with EL1.	45
5-4	CV measurements of 2-layer electrodes with EL2.	46
5-5	CV measurements of 2-layer electrodes with EL3.	47
5-6	MATLAB integration of CV-curve.	48
5-7	Calculations of the areal capacitance of the printed devices. . .	48
5-8	CV-measurement over a large number of cycles.	49
5-9	Comparison of CV-measurements over time.	50
5-10	EIS measurements of 1-layer electrodes with EL1.	51
5-11	EIS-measurements of 2-layer electrodes with EL1.	51
5-12	EIS-measurements of 4-layer electrodes with EL1.	52
5-13	EIS measurements of 2-layer electrodes with EL2.	53
5-14	EIS measurements of 2-layer electrodes with EL3.	53
5-15	Summary of the ESR recorded for the measured devices. . . .	54
5-16	Calculations of the areal capacitance of the printed devices. . .	55
5-17	Results from stretchability tests performed at Tampere University (TAU). The figures show the normalized resistance as a uniaxial strain is applied.	56
5-18	Images from SEM showing the morphology of the PEDOT:PSS electrode material fabricated by DIW.	57
6-1	The current place of this work and future outlooks for further development.	59

List of Tables

2.1	Summary of the most common materials used for printed stretchable MSCs [23, 24, 28].	19
4.1	Printing parameters and their effects on print quality.	34
4.2	Chemicals used for experiments.	35
4.3	Main compositions of the formulated electrolytes.	36
4.4	Overview of the fabricated devices used for measurements. . .	37
6.1	Capacitance values of fabricated devices.	65

List of Abbreviations

AC	Activated Carbon
AM	Additive Manufacturing
BP	Black Phosphorous
CNT	Carbon Nanotube
CV	Cyclic Voltammetry
DIW	Direct Ink Writing
EDL	Electric Double Layer
EDLC	Electric Double Layer Capacitor
EIS	Electrochemical Impedance Spectroscopy
FDM	Fused Deposition Modeling
GCD	Galvanostatic Charge-Discharge
GPE	Gel Polymer Electrolyte
IDE	Interdigitated Electrode
IHP	Inner Helmholtz Plane
IPA	Isopropyl Alcohol
LM	Liquid-Metal
MOF	Metal-Organic Framework
MSC	Microsupercapacitor
OHP	Outer Helmholtz Plane
PDMS	Polydimethylsiloxane
PE	Printed Electronics
PEDOT	Poly(3,4-ethylenedioxythiophene)
PEG	Polyethylene Glycol

PEO	Polyethylene Oxide
PSS	Polystyrene Sulfonate
PSSH	Poly(4-styrene Sulfonic Acid)
PVA	Polyvinyl Alcohol
SC	Supercapacitor
SEM	Scanning Electron Microscopy
STEC	Stretchability and Conductivity Enhancer
TPU	Thermoplastic Polyurethane

1 | Introduction

1.1 Background

Printed Electronics (PE) is an emerging technology in the field of electronics. While traditional silicon technologies are predominant in electronics manufacturing, PE has several advantages. The most important advantage is the relatively simple and cost-effective fabrication methods that are involved in printing electronics [1]. The technology also benefits from having more versatility in terms of available substrate materials. InkJet printing is a well-established technique for printing the two-dimensional electrodes of a Supercapacitor (SC). However, it is a time-consuming printing process if thick structures are required since it is based on jetting small droplets, typically in the pL range [2]. By using other techniques such as Direct Ink Writing (DIW), it is possible to enable printed structures with thicknesses in the range of 100-200 μm with relatively short printing times.

Another promising feature of PE is that it opens up the possibility of producing stretchable electronics. Stretchability in this context refers to the ability of an electronic component to retain the performance while a large mechanical strain is applied. Traditional electronics have relied heavily on silicon substrates and metal interconnects, while PE offers the ability to print stretchable conductive materials on substrates that can be elastically deformed [2]. This opens up a new range of applications such as electronics integrated in clothes or in smart patches that can be placed on the human body. For stretchable electronics to become fully realized, there is a need to develop stretchable energy storage devices [3].

This project will be focused on two parts of this process:

- formulating conductive, intrinsically stretchable inks and electrolytes
- fabricating intrinsically stretchable energy storage devices using DIW

This will serve as a proof-of-concept for fully stretchable devices using simple additive manufacturing techniques.

1.2 Problem

Research in printed stretchable energy storage devices has been growing rapidly. The research has been devoted to DIW of energy storage devices and to stretch-

able electronics respectively. However, combining both technologies into a single method still remains a novel approach, although some research has been conducted on DIW of intrinsically stretchable SCs with promising results [4]. The main difficulty is the development of materials for electrodes and electrolytes that are compatible and have sufficient electrochemical properties. The need for the materials to be stretchable is another obstacle. The problem that will be researched in this thesis is:

The viability of Direct Ink Writing for fabricating intrinsically stretchable EDLCs.

1.3 Purpose

The purpose of this thesis is to investigate the method of DIW of intrinsically stretchable energy storage devices. The thesis is also intended to provide the reader with information about state-of-the-art advancements in the development of stretchable energy storage devices and what the applications for such technologies will be in the future. The outcome of the project will be a quantitative evaluation of SCs fabricated by DIW, both with respect to similar technologies as well as their electrochemical performance when a mechanical strain is applied.

1.4 Goal

The objective of the work in this thesis is to be a proof-of-concept of a simple DIW technique for intrinsically stretchable SCs. The goals of the project are to:

- Formulate functionalized and intrinsically stretchable inks and electrolytes.
- Develop a reliable DIW process to fabricate SCs using the formulated materials.

The results from reaching these goals will include:

- Results from measurements of the stretchability of the formulated materials.
- Data from electrochemical characterization, displaying the performance of fabricated devices.

1.5 Methodology

An important part in scientific research is the choice of an appropriate methodology. A research methodology can be described as the motivation of the choice of methods. The validity of a research project largely depends on the appropriate motivation of the methodology. Research can roughly be categorized as either quantitative or qualitative [5]. The methodologies in quantitative research rely on using methods that allow for either direct or indirect measurements. This is distinguished from qualitative research which primarily uses observations of non-numerical data.

Figure 1-1 shows the process steps for quantitative research. Methods comprise the specific actions taken to gather results, whereas methodology includes all of the steps. If a research is lacking in any of the described steps, it can compromise the validity and conclusions from the results. Steps 1-3 relating to this thesis will be described in the following subsections, while steps 4-8 are presented in Chapter 3.

The methodological approach chosen for this project was selected to demonstrate the feasibility of the proposed technology. This will be achieved by using well-established characterization methods described in Chapter 3.2. These results can then be quantitatively compared to other similar technologies. This approach provides an accessible means to demonstrate the performance of the printed devices in a time frame that is within the scope of the thesis.



Figure 1-1: Schematic description of the quantitative research process.
Adapted from [5].

Philosophical assumptions

The basis for any research project are the *philosophical assumptions* on which it rests. These will serve as a guidance for all of the subsequent steps taken. The assumptions can be based on an objective (*Positivism*), realistic (*Realism*), interpretive (*Interpretivism*) or critical (*Criticism*) standpoint. This will affect how researchers approach the specific research topic [5].

Experimental and exploratory research should be based on objective philosophical assumptions, that there exists an objective reality that researchers can discover through logical reasoning and by using deductive inference. This thesis is based on the philosophical assumption that DIW has the potential of becoming a valid method for creating cost-effective, intrinsically stretchable MSCs. The experimental results in this thesis will be used to either lower or increase the validity of this assumption.

Research methods

Once research goals have been clearly defined, the next step is to form a plan or procedure to reach those goals. This is accomplished by choosing an appropriate *research method*. This can be thought of as a recipe describing the necessary steps to go from start to finish of a research project in a scientifically valid manner. The most common research methods are Experimental, Descriptive, Qualitative, Analytical, Fundamental/Basic, Applied, Conceptual and Empirical [5]. The chosen research method for this thesis is an experimental one, with the motivation that the research goal is to prove the feasibility of stretchable SCs fabricated by using DIW, and also to investigate how their electrochemical performance can be improved. This research is somewhat exploratory, necessitating the use of experimental methods. The experimental research method also allows to investigate the effects of background variables on the outcome of the devices, and change them accordingly.

Research approach

A research approach describes what reasoning is used for drawing conclusions from results [5]. The two main categories of research approaches are *deductive* and *inductive*. A deductive approach starts by formulating a hypothesis, and makes predictions of observable consequences given that the hypothesis is correct. The outcome of experiments and analysis of results will either increase or decrease the confidence in the hypothesis. The inductive approach is somewhat the inverse. Observations of data or patterns are used to make

a hypothesis and to create a theory that is valid given the data. Figure 1-2 highlights the characteristics and differences between the two approaches.

The approach in this thesis is one of deductive inference. The hypothesis is that *stretchable MSCs with electrochemical properties comparable to previously reported results can be fabricated by DIW*. This is operationalized by using the standard methods for electrochemical characterization. The expected outcome of these measurements are values of capacitance and energy density that will be compared to those found in literature of previous similar work.

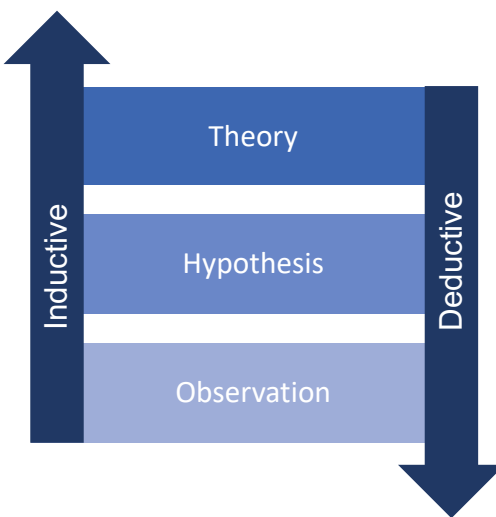


Figure 1-2: Simplified description of different research approaches.

1.6 Outline

This thesis is divided into three main sections:

1. **Chapter 2: Theoretical background to the project.** This section covers the most essential topics for the reader to understand the concept of supercapacitors, the main challenges involved in the technology and what methods will be used for the presented topic. The methodology that was used to reach the goals of the project are also presented in this section.
2. **Chapter 3: The experimental body of the project.** All of the experimental work that was performed to research the proposed topic is presented in this section. The section contains information regarding

the general methods used to fabricate the devices as well as detailed descriptions of the work that was carried out.

3. **Chapter 4 & 5: Results and conclusions that are drawn from the results.** In the section, all results from characterization and the experimental investigations are presented to the reader, together with the main conclusions from the results.

2 | Theoretical background

2.1 Printing technology in electronics

This section aims at giving the reader a brief overview of PE (Printed Electronics). This will serve as a theoretical background to give better understanding of the experimental procedure and the importance of this project.

Overview

Printed electronics is the name used for a collection of electronics manufacturing techniques that involve printing methods. PE is a field of technology that is growing because of the relatively simple manufacturing process. Traditional methods involve complex process steps, including cleanroom fabrication and expensive materials. PE also has the additional advantages of being versatile and compatible with a wide variety of materials and substrates [1]. The ability to manufacture electronics using less expensive materials and tools makes the technique suitable for applications where the requirements on performance are less important than low cost. The applications for PE are normally divided into the categories: sensors, RFID tags, photovoltaic cells, batteries, lighting and displays [2].

A useful definition of PE is the use of any printing method to produce electronic circuits or components on a variety of substrates. The first printed electronics were limited to printing electrical circuits on rigid printed circuit boards [2]. These techniques are still used today, for example printing current collectors using silver on solar cells, and have advanced to printing on flexible substrates such as thin plastic films. This is the most widespread use of PE today. The next major development in PE is likely to be the development of stretchable electronics, using both substrate and printing materials that can be strained without losing their performance [6]. This evolution of PE is described in Figure 2-1.

Advantages and challenges of printed electronics

Advantages

There are two main driving forces behind the development of PE. Firstly, the possibility to manufacture electronic components at a cost that is lower than that of traditional methods [1,2]. It has been estimated that the cost of PE will

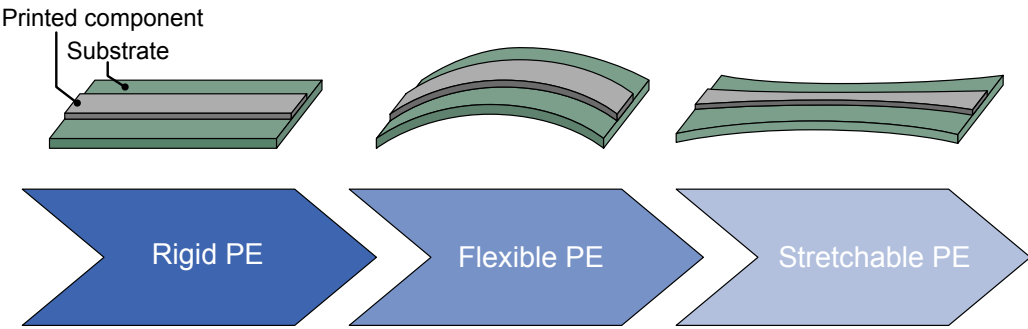


Figure 2-1: Evolution of printed electronics.

be several orders of magnitude lower than that of silicon technologies per unit area. Not only are the materials cheaper in general, but the tools necessary for manufacturing are also less capital intensive.

Secondly, PE offers flexibility in the choice of substrate materials that silicon technologies can not. Many of the chemical and physical processes that are involved in silicon technologies are not compatible with polymer substrates. Furthermore, the deposition methods rely largely on using metals and the possibility to deposit other conductive materials are limited. PE will serve as a low-cost manufacturing process for purposes where traditional methods are not feasible, either by being inaccessible due to the cost or by being limited by processing factors.

Challenges

The main challenge facing PE is the development of new materials [1]. In order to serve as a complement to traditional methods, the materials must meet several requirements, such as deposition at low temperatures and compatibility with other materials. They also need to be easily processed in liquid form, which makes the development of suitable inks an important aspect.

A technical challenge facing PE is to manage the printing variability and to ensure the repeatability of the prints [1, 7]. The printing variability can be categorized as material variability and process variability. A difficulty with printing fluids is that changes in the homogeneity of the material can affect the electrical properties. As most printed electronics rely on using polymers as the retaining matrix for the conducting material, factors such as heat, exposure to UV-light and humidity can have an affect on the print quality.

Stretchable electronics

The technological evolution of flexible electronics spans more than 4 decades [8]. Flexible and light-weight solar cells and flexible LED-screens are two of the most important applications for the technology. However, flexible electronics are designed to withstand a small degree of strain. There has been a growing interest in using electronics for applications where a large degree of strain tolerance is necessary. Figure 2-2 shows one application for stretchable electronics. Health monitoring is believed to be a major application involving

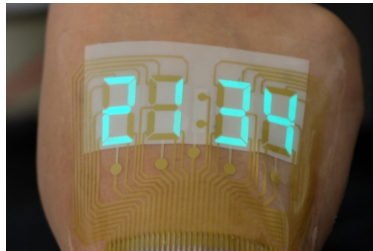


Figure 2-2: Stretchable luminescent screen. Reprinted with permission from [9]. Copyright (2019) American Chemical Society.

stretchable electronics. The concept of *lab-on-skin* has been introduced in a recent review paper. The term refers to devices with physical properties similar to those of the human skin. It was noted that it is difficult to imagine this technology without incorporating energy storage devices such as batteries or supercapacitors [10]. Figure 2-3 shows the three methods of attaching lab-on-skin devices.

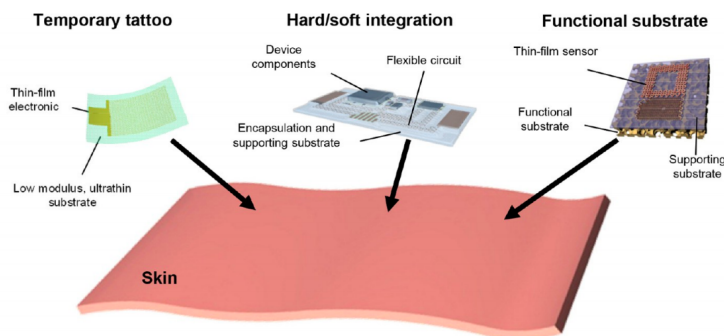


Figure 2-3: The main methods of incorporating electronics on human skin. Reprinted with permission from [10]. Copyright (2017) American Chemical Society.

2.2 State-of-the-art printing techniques

Additive Manufacturing (AM) are processes in which material is added to create a structure. This section will describe the most commonly used AM solutions in electronics manufacturing. Figure 2-4 shows schematically the three described printing techniques.

Screen printing

Screen printing is a printing technology that can be used with simple tools. It uses a mesh with the desired pattern made from a material blocking the ink [1]. Ink is placed on top of the mesh and is applied using a squeegee. The capillary forces produce a negative image of the pattern as it comes in contact with the surface. Screen printing has been used in electronics manufacturing for many years and serves as the main method for replacing etching techniques to produce thin lines of either metal or organic materials. Line thicknesses of $<100\text{ }\mu\text{m}$ are reproducible with a single pass and high aspect ratios can be achieved [2]. However, a resolution of less than $30\text{ }\mu\text{m}$ is difficult to achieve [11].

The main drawback is that screen printing is not a contactless technique. This creates difficulties in alignment when stacking layers of material to create thicker patterns, leading to a trade-off between resolution and thickness. A second drawback is the relatively high material waste related to the printing process [12], as well as the need for multiple masks. There is also a tendency for the material to spread out, deteriorating the pattern [11].

InkJet printing

InkJet printing is a contactless and maskless printing technique in which small droplets of ink are ejected through a nozzle attached to a printhead. This method is commonly referred to as drop-on-demand [12]. The printhead follows a predetermined schedule according to the desired print. InkJet printing has gained a strong foothold in PE due to its high resolution. Line thicknesses of $10\text{ }\mu\text{m}$ are available [12]. The technique has low constraints on the materials that can be used for printing. Inkjet printing has been used to print flexible SCs with high power densities and large areal capacitance [12, 13].

The major disadvantage of InkJet printing is that it is difficult to achieve a thick layer of material. Even when multiple layers are added, reaching pattern thicknesses above $10\text{ }\mu\text{m}$ is time-consuming, which makes the throughput relatively small compared to other printing methods.

DIW (Direct Ink Writing)

The latest addition to printed electronics is the technique commonly referred to as Direct Ink Writing. The name DIW will be used for the purpose of this thesis to describe the process of printing successive layers of material to form freestanding 3D structures.

DIW as a technology has gained attention due to its simple manufacturing process, high printing speed and high degree of repeatability [1]. The method can be described as printing individual 2D layers that are assembled vertically to produce a 3D structure. Softwares that can convert CAD models into such stacked structures are readily available. This method of stacking and merging successive layers of material is also commonly referred to as Fused Deposition Modeling (FDM), a process in which a thermoplastic is melted, printed through a nozzle and left to cool down. The technology has since then been extended to include printing other types of materials, such as viscous fluids. This extension has opened up the application of 3D bioprinting.

DIW of viscous fluids has also allowed for printing of electronic patterns and components with greater thicknesses compared to other techniques. One technique is to print a mold which can be used to cast electronic components [11]. The technique can also be used for printing the electronic components directly. This has been used to print interconnects, antennas, strain sensors and passive components [14]. It can also be used as a replacement for soldering when connecting components to a temperature-sensitive substrate.

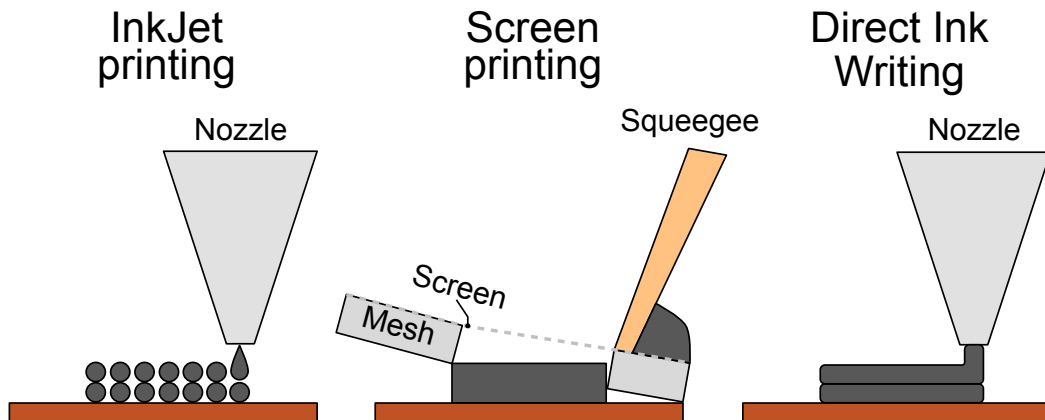


Figure 2-4: Schematic description of three common AM methods.

2.3 Printed electronics in energy storage

This section provides a theoretical background to the fundamental principles of SCs. The goal is to provide the reader with a perspective on the purpose of printed energy storage devices.

Microsupercapacitors

Much attention has been brought to the development of novel energy storage technologies. There are two main features common to all energy storage devices: energy density (unit W kg^{-1}) and power density (unit Wh kg^{-1}) [12,15]. Batteries typically have a high energy density. However, the charge and discharge of the energy is relatively slow. A capacitor has somewhat opposite characteristics of a battery in terms of performance. A capacitor will charge and discharge quickly, giving it a superior power density. This trade-off behavior between power density and energy density can be illustrated in a so-called Ragone plot shown in Figure 2-5.

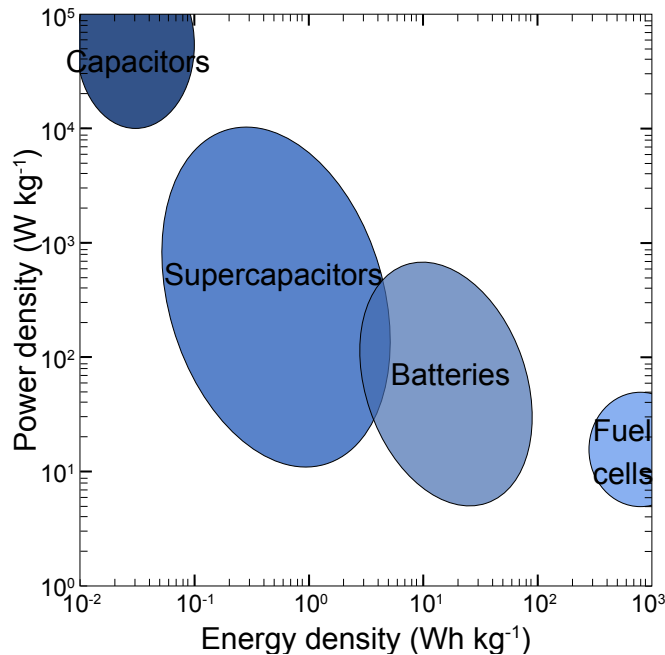


Figure 2-5: Ragone plot displaying the trade-off between power density and energy density. Adapted from [12, 15].

A capacitor fundamentally consists of two oppositely charged electrodes with a dielectric between. The capacitance of a capacitor can be calculated using the equation

$$C = \varepsilon \frac{A}{d} \quad (2.1)$$

where ε is the permittivity of the dielectric material separating the electrodes, A is the area of the electrodes and d the separation between the electrodes. The physical attributes of the capacitor are essential: a large area and a small spacing gives a large capacitance. A SC is a capacitor that has energy storage capabilities typically several orders of magnitude higher than that of a traditional capacitor [15]. A miniaturized SC is commonly referred to as a Microsupercapacitor (MSC). For MSCs, the capacitance is usually reported as either areal capacitance (unit F cm^{-2}) or specific capacitance (unit F g^{-1}) depending on the application.

Research on printed MSCs has mainly been focused on InkJet printing and screen printing because of their flexibility in choice of material and high resolution. Screen printing was used to print interdigitated MSCs on a flexible PET substrate using an ink composed of MnO_2 and onion-like carbon [16]. The device exhibited a maximum capacitance of 7.04 mF cm^{-2} and retained 80% of its capacitance after 1000 cycles. In another article, a process for InkJet printing of MSCs was developed [12]. The devices were fabricated using exfoliated graphene electrodes together with an electrolyte based on nano-graphene oxide. Results revealed an areal capacitance of $313 \mu\text{F cm}^{-2}$. In both studies, MSCs were fabricated on flexible substrates.

Electric Double Layer Capacitor (EDLC)

Supercapacitors can be of different types, the most common of which is the Electric Double Layer Capacitor (EDLC). The basic parts of an EDLC are described in Figure 2-6. Two electrodes covered with an electrolyte are charged by applying a bias. The outermost atomic layer of the electrode becomes polarized and attracts ions of opposing charge. This forms an Electric Double Layer (EDL) at the electrode-electrolyte interface [12]. A simplified equivalent series model of the EDLC is presented in Figure 2-6. The total capacitance of the cell in the figure can be calculated as

$$\frac{1}{C_{\text{tot}}} = \frac{1}{C_1} + \frac{1}{C_2} \quad (2.2)$$

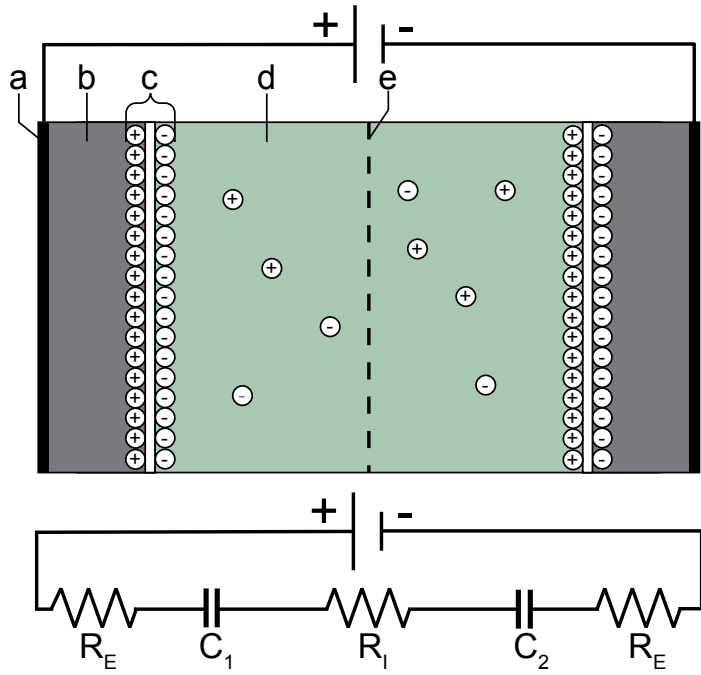


Figure 2-6: Top figure: Parts of a charged EDLC: (a) current collector, (b) electrode, (c) electric double layer, (d) electrolyte, (e) separator. Bottom figure: Equivalent electrical circuit for an EDLC.

If the electrodes are symmetrical, the capacitance of either electrode is half that of the entire cell. It is thus important to present capacitance values as either *cell capacitance* or *electrode capacitance* [15].

The charge separation occurs at the innermost layer or Inner Helmholtz Plane (IHP), where the entire area of the electrode is covered by ions of opposite charge. At the Outer Helmholtz Plane (OHP), a second distinct layer of both positively and negatively charged ions is formed. The diffuse layer starts at the OHP. The Stern layer contains both the IHP and the OHP [15]. This is presented in Figure 2-7a. Since the capacitance is directly related to how many ions are contained in the EDL, increasing this area is critical. This is described in Figure 2-7b, which shows an electrode of a porous material containing a large number of ions. The ions can penetrate deep into the material and the EDL becomes significantly larger.

When the bias is reversed and the capacitor is discharged, the ions in the Stern layer diffuse back into the diffuse layer. The distance that the ions in

the Stern layer have to diffuse is at a length scale of tens of Å. Analogous to Equation 2.1, d becomes essentially the thickness of the Stern layer. This is the main reason why EDLCs have much higher energy storing capabilities than conventional capacitors [15]. Because of the short diffusion distance, the charge/discharge cycle is also shorter for EDLCs.

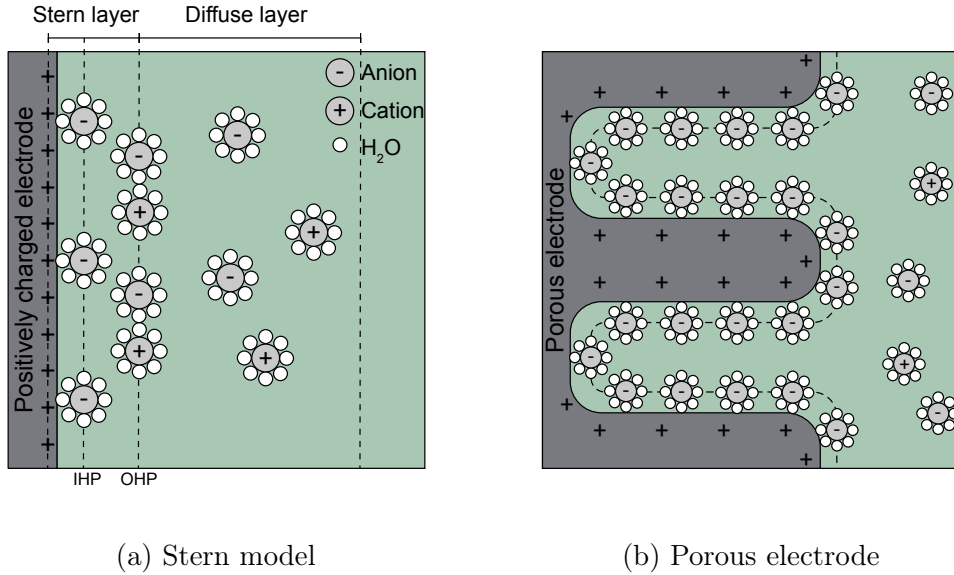


Figure 2-7: Detailed description of the basic mechanism of an EDLC. Adapted from [15].

The two main factors that determine the performance of an EDLC are the active electrode surface area, which determines the capacitance, and the electrolyte properties, which determines the potential window [15]. Using porous electrode materials is the most common way of surface area increase by ways of material engineering. Carbon based materials such as Activated Carbon (AC) and Carbon Nanotube (CNT) are some of the most well-researched. These materials offer the advantage of high electrical conductivity and high porosity. Using graphene based materials has become increasingly interesting for energy storage applications. A second approach is to design device patterns of a large active area. Figure 2-8a shows the main components and a schematic layout of a typical EDLC. The device consists of an Interdigitated Electrode (IDE) pattern covered by an electrolyte. The overlapping electrode fingers increase the total device area. A current collector is used to decrease the total resistance when performing measurements on the contact pads.

DIW-fabricated energy storage devices

There has been a growing interest in using DIW for printed electronics. DIW has similar flexibility in terms of substrate material and printed materials as other techniques, with the additional advantage of being able to print thicker structures. A sub-millimeter Li-ion battery was printed using a simple DIW method [17]. The interdigitated electrodes were printed with several layers on a current collector and immersed with a liquid electrolyte as shown in Figure 2-8b. Results from the measurements showed power and energy densities comparable to other reported literature values.

In another study, a DIW process has been used to print a SC [18]. The material used for the electrodes were based on an AC slurry that was printed on a flexible substrate. A maximum capacitance of 68.7 mF was measured. It was concluded that the technique could serve as a method for fabricating several functional elements using only one process. A similar setup was used to print CNT-based MSCs [19]. Interdigitated electrodes were printed on a glass substrate. The fabricated device exhibited a maximum capacitance of 4.69 mF cm^{-2} , which according to the study is comparable to that of non-printed devices.

Several other studies using DIW to produce interdigitated electrodes based on CNTs, graphene oxide, graphene and AC show similar electrochemical performance [20–22]. The approach in the research is relatively similar, using DIW to print the structures on a current collector and applying a liquid electrolyte.

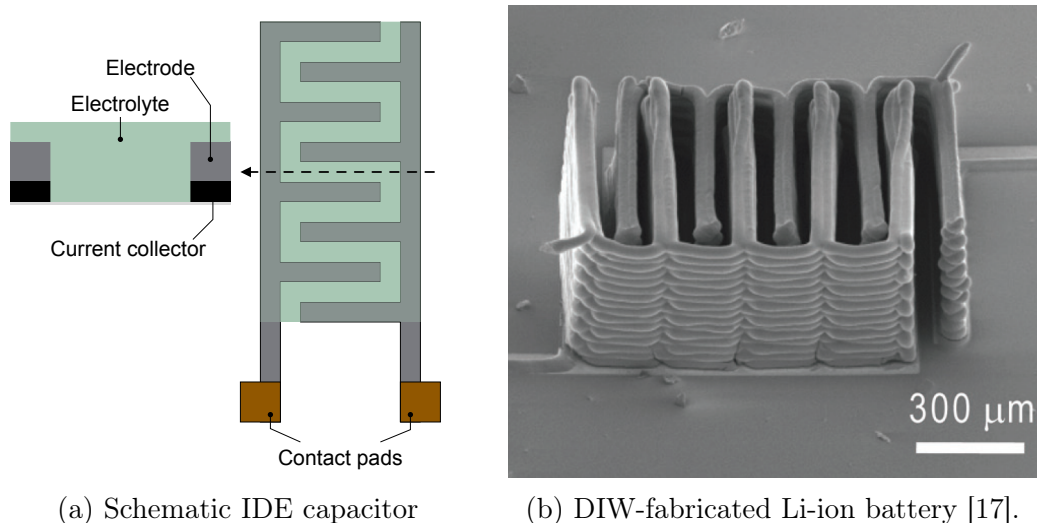


Figure 2-8: Common designs for high-performance energy storage devices.

2.4 Stretchable microsupercapacitors

The next step forward in energy storage applications will be to print fully stretchable electronics. Stretchability in this context is different from elasticity. Elasticity refers to the property of being elastic, whereas a stretchable material needs to be elastic as well as retain the specific performance at an arbitrarily defined degree of strain. This section covers the concept of stretchable MSCs and the most recent developments in the field.

Materials

Electrode materials

The most common materials used for electrodes in stretchable MSCs are carbon-based materials, metal oxides and conducting polymers. Other less common materials such as MXenes, Black Phosphorous (BP) and Metal-Organic Framework (MOF) are also of interest [23, 24]. The most common materials are summarized in Table 2.1. Embedding the aforementioned materials in a stretchable matrix is necessary. For printed electrodes, the typical procedure is to formulate an ink with the desired rheological and electrical properties. The ink typically contains fillers, solvents, binders and additives [23] which serve different purposes. As the ink dries, it will form a network of conductive material embedded in the stretchable retaining matrix.

Using metallic or carbon-based electrode materials provides the highest electrical conductivity. However, a large amount of strain tends to separate the conductive components and reducing the overall conductivity. A solution is to use a conductive polymer as the active electrode material. Consisting of long polymer-chain networks, conductive polymers can withstand some strain with retained electrical performance.

The band structure of a conductive polymer is more similar to that of an insulator than that of a metal [25]. This is also suggested by the fact that the conductivity does not increase with decreasing temperatures. The explanation for this is a tendency for charge carriers to be localized in a disordered system [26]. The band gap can however be adjusted by the addition of dopants, such that the polymer becomes either *n*-type or *p*-type, resulting in an insulator-to-conductor transition [25, 26]. The details of the mechanism of doping is different from that of semiconductors. Instead of substitutionally doping the material, electrons and holes reside interstitially between bonds in the polymer backbone and subsequently fill up states in the conduction band.

PEDOT:PSS is a commonly used conducting polymer for organic electron-

ics [27]. The polymer is a complex polyelectrolyte that is composed of Poly(3,4-ethylenedioxythiophene) (PEDOT) and Polystyrene Sulfonate (PSS) [28]. The conductivity of intrinsic PEDOT:PSS is relatively low (typically $>0.1 \text{ S cm}^{-1}$), however an increase of conductivity of several orders of magnitude has been achieved by adding a secondary dopant [28, 29].

Electrolytes

An important aspect of stretchable MSCs is the properties of the electrolyte. A solid-state (gel) electrolyte is commonly used for printed MSCs [23], as opposed to using a liquid electrolyte. A separator between the electrodes is redundant when using a gel electrolyte, and packaging is less demanding. The use of a Gel Polymer Electrolyte (GPE) is among the most promising methods for stretchable MSCs, due to the high ionic conductivity in the range 10^{-4} - $10^{-1} \text{ S cm}^{-1}$ [24]. The GPEs can be categorized as either aqueous, organic or ionic liquid-based. All of the categories have the advantages of displaying a high ionic conductivity, low cost and being relatively non-hazardous to the environment [23]. Aqueous GPEs suffer from a narrow potential window, which can be solved by adding a plasticizer such as propylene carbonate, dimethyl formamide or ethylene carbonate. Ionic-liquid based GPEs offer extra advantages such as non-volatility and superior mechanical properties. They are also less corrosive and more stable, which makes them suitable for printing applications.

As the retaining matrix for the electrolyte, extensive research has been devoted to Polyvinyl Alcohol (PVA). The polymer has desirable properties such as being non-toxic, highly hydrophilic and relatively inexpensive. In an article, researchers presented results from an intrinsically stretchable supercapacitor using a PVA-H₃PO₄ GPE [30]. According to the authors, H₃PO₄ is known to act as plasticizer. The effect of the H₃PO₄/PVA ratio on the strain tolerance was studied. It was concluded that at a ratio of 1.5:1, the strain tolerance reached a maximum, with higher ratios leading to a loss of stretchability. At said ratio, the electrolyte displayed a conductivity of $3.4 \times 10^{-3} \text{ S cm}^{-1}$ and could withstand a uniaxial strain of 410% before rupture.

Substrates

Polymers are the predominant material used as substrates for stretchable MSCs. Silicone and specifically Polydimethylsiloxane (PDMS) substrates have been used for printed MSCs, displaying a high strain tolerance [23]. Furthermore, PDMS is inexpensive and biocompatible [27], making it a suitable choice for environmentally friendly energy storage devices. PDMS does however have

hydrophobic properties. This can be overcome by pre-treating the substrate, either chemically or by using plasma [23]. Other polymer substrates such as Thermoplastic Polyurethane (TPU) and styrene-block-isobutylene-block-styrene have been reported to display great stretchability [30].

Table 2.1: Summary of the most common materials used for printed stretchable MSCs [23, 24, 28].

Component	Category	Material
Active material	Carbon-based	Graphene, AC, GO, CNT
	Metal oxides	NiO, CoO, MnO ₂ , V ₂ O ₅
	Conducting polymer	PTH, PPy, PANI, PEDOT:PSS
	Other	MXene, BP, MOF, LM
Electrolyte	Acid	H ₃ PO ₄ , H ₂ SO ₄ , Na ₂ SO ₄ , PSSH
	Salt	KOH, LiCl
Plasticizer	Aqueous	H ₂ O
	Organic	Glycerol, Xylitol, Triton X-100
Binder	Polymer	PVA, PDMS, PEO, PEG
Substrate	Polymer	TPU, PDMS, Elastomers
	Metal	Stainless steel mesh

2.5 Approaches to stretchable MSCs

Stretchable electronics in this context refers to electronic components and devices that can be strained and deformed to a large extent without significant reduction of performance. What degree of strain is considered significant can vary from a few percent to a few hundred percent. There are several viable approaches that result in two categories of stretchable MSCs: structurally stretchable or intrinsically stretchable MSCs [23, 31].

Structurally stretchable MSCs

Structurally stretchable patterns can be likened to origami-like structures, in which the pattern is folded or curled up in its nominal state. Once stretched, it will unfold without straining the material as described in Figure 2-9. In the figure, the wave-shaped electrode material is not stretchable, but when applying a strain ΔL , the pattern will unfold to form a flat surface. This is a viable approach, however the performance of the device is limited by two factors:

- mismatch in strain tolerance of the electrode material and the electrolyte.
- the pre-strain of the material.

The nature of this approach creates difficulties for reaching high device densities as well as making it more difficult to package the out-of-plane patterns [31].

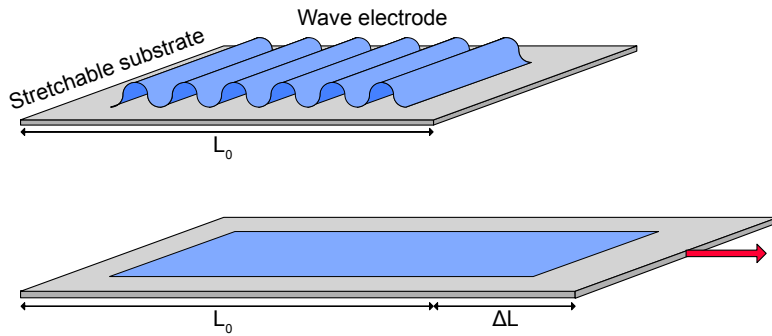


Figure 2-9: Basic idea behind a structurally stretchable electrode.

A study was conducted in which a polypyrrole/black-phosphorous oxide was deposited on a CNT film [32]. The electrodes were fabricated in a hon-

eycomb pattern which could be strained to 2000% before affecting the performance. A similar technique was used in another study, in which researchers fabricated an array of MSCs on a stretchable honeycomb-shaped PDMS substrate [33]. The devices displayed no significant reduction in performance up to 275% uniaxial strain. This highlights the potential of designing innovative macrostructures that allow substantial strain.

However, most research has been devoted to fabricating stretchable structures on a micro scale. This strategy was realized in a study in which researchers used crumpled graphene paper electrodes to fabricate supercapacitors [34]. Graphene papers were produced and bonded onto a compliant pre-stretched substrate. The supercapacitor was prepared by adding a liquid PVA-H₃PO₄ electrolyte onto one crumpled graphene paper electrode and drying before bonding it to the other electrode. The device displayed a maximum capacitance of $\sim 49 \text{ F g}^{-1}$ and retained this capacitance at an uniaxial strain of 150% and areal strain of 300%. Although the electrode material could withstand an areal strain of 800% without decrease in its electrochemical performance, the electrolyte was limited to 300% areal strain before failure.

In a similar study [35], researchers grew Au-CNT forest electrodes which were transferred onto a pre-stretched elastomer substrate as shown in Figure 2-10. This allowed the microstructure of the electrodes to fold into a crumpled structure. The device displayed a maximum capacitance of 26.33 mF cm^{-2} . At an areal strain of 800%, the capacitance retention was $\sim 56\%$. Similar attempts using buckled CNT films have been demonstrated but with tolerance to strain in the range of 30-120% before impacting the device performance [36, 37].

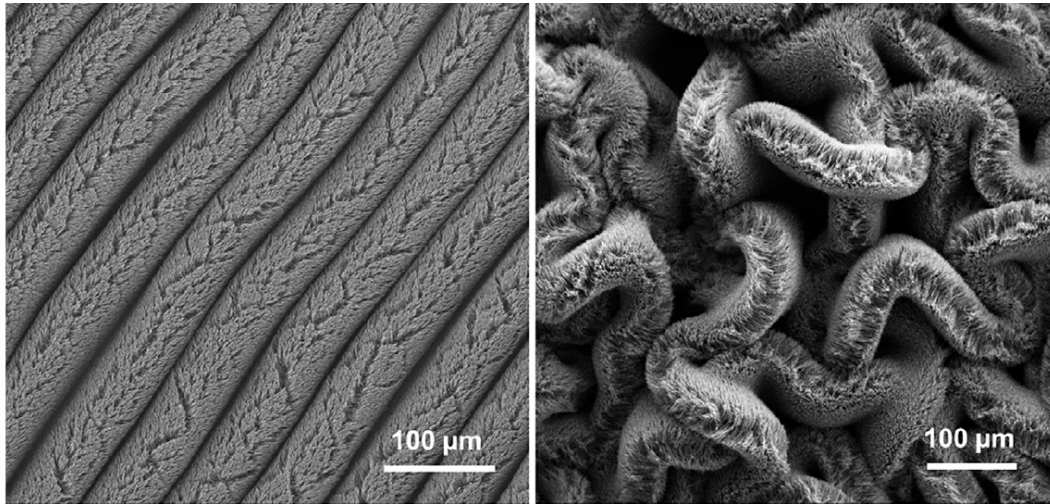


Figure 2-10: Example of a structurally stretchable electrode. Courtesy of [35].

Intrinsically stretchable MSCs

In attempts to circumvent the inherent limitations in structurally stretchable MSCs, there has been research devoted to intrinsically stretchable MSCs. These belong to a category of devices of which the stretchability relies on inherent properties of the materials rather than geometrical structures. Figure 2-11 shows a schematic description of the stretchability mechanism. Conducting polymers belong to the most promising materials for the application [31]. However, there is normally a trade-off between conductivity and stretchability. This is due to the fact the a high degree of crystallinity improves conductivity but impedes the elastic behavior of the material.

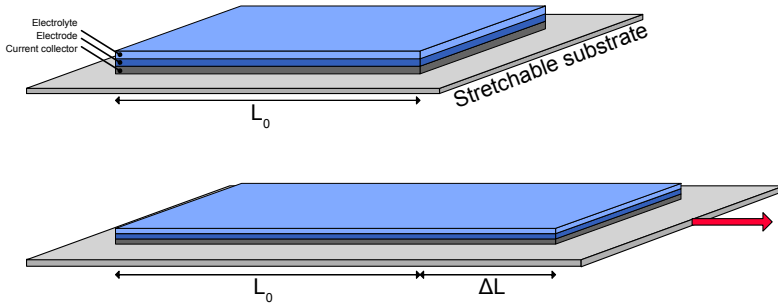


Figure 2-11: Basic function of an intrinsically stretchable electrode.

Several studies have been carried out to study intrinsically stretchable electrode materials. In one study, researchers prepared an ink using Liquid-Metal (LM) droplets suspended in a silicone elastomer matrix [38]. The LM ink was printed using DIW to form a circuit and subsequently pressed and freezed to activate the LM droplets. The circuit was printed on a silicone elastomer substrate. The stretchability was tested by applying the circuits around the fingers of one hand and bending the fingers in different ways while measuring the conductivity. The researchers concluded that the ink displayed a sufficient conductivity, however it also displayed a significant increase in resistance when strained. This behaviour is ideal for applications such as strain-gauges, however it is not ideal for electrode materials.

One group of researchers showed the feasibility of fabricating intrinsically stretchable MSCs by laser patterning [39]. The fabricated interdigitated device retained 38% of its initial capacitance when stretched to 80% in the direction parallel to the electrode fingers. In another study, researchers coated a polymer fiber with alternating layers of CNT sheets and PVA-H₃PO₄ elec-

trolyte [40]. The fiber capacitor retained >95% of the initial capacitance after a strain of 75% was applied for 100 cycles. At 100% strain the device displayed a significant decrease in capacitance.

To investigate less commonly used materials, researchers attempted to fabricate MSCs based on a nanocomposite gel using DIW [4]. The active material in the gel consisted of Ti_3C_2Tx nanosheets, manganese dioxide and silver nanowires, and fullerenes. DIW was used to print interdigitated structures and a freezedrying technique allowed for a unidirectional crystal formation within the electrodes. The device was covered with a PVA-KOH GPE. The results revealed a maximum capacitance of 216.2 mF cm^{-2} . According to the authors, the capacitance of the device outperforms all previously reported values for stretchable MSCs. At a uniaxial strain of 50%, the capacitance retention was ~80%.

Intrinsically stretchable MSCs are especially interesting for printing techniques because they offer simple and inexpensive methods of fabrication. The main requirements for electrode materials in general are high electrical conductivity and large surface area, while electrolytes need high ionic conductivities. For printed MSCs, there are further requirements. Processability, performance and reliability over time are important properties that need to be considered [40].

2.6 Properties of PEDOT:PSS

Morphology

In the field of organic electronics, PEDOT:PSS belongs to the most commonly used materials. However, the knowledge of the fundamental physics governing the conduction is still limited. The chemical formula and theoretical morphology of PEDOT:PSS is depicted in Figure 2-12. Long chains of PSS form bundles that are accompanied by shorter PEDOT chains [28]. In water, a gel is formed with PSS-rich domains and clusters of PEDOT:PSS-rich domains. PEDOT:PSS has varying mechanical properties depending on the ratio of the two polymers. Factors such as humidity, additives and processing conditions also have a strong impact on the behavior of the material.

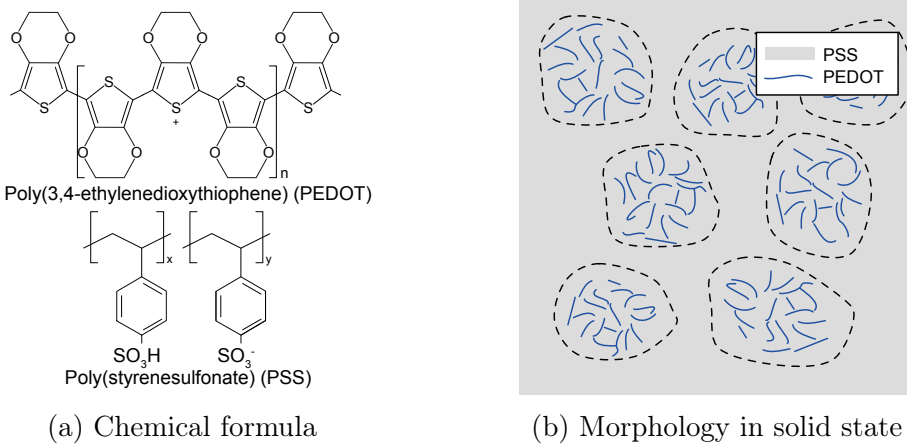


Figure 2-12: Specific properties of PEDOT:PSS.

Capacitance

In an article, the capacitive behavior of PEDOT:PSS was investigated [41]. The motivation for the study was to investigate the commonly accepted view that the voltammograms of conductive polymers are governed by pseudocapacitive processes. The experimental work was performed by doing measurements on PEDOT:PSS/Au electrodes in an N₂ atmosphere using a 0.1 M KCl electrolyte. Two models of the situation were produced: one in which a 1-phase homogenous PEDOT:PSS material was simulated as described in Figure 2-12b and one in which 2-phases of distinct PEDOT-rich and PSS-rich domains are presented as in Figure 2-13. The results showed that the modeled 2-phase

material could explain the capacitance by introducing electric double layers forming between grains of the two phases without invoking faradaic reactions. This behaviour is similar to that of a porous electrode material. Thus, the authors argue that the key to understanding capacitive behavior of PEDOT:PSS lies in the morphology.

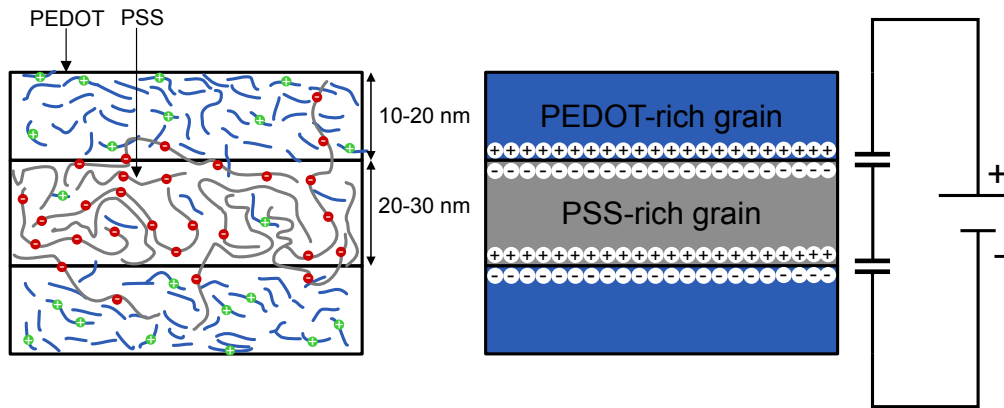


Figure 2-13: Modeling of PEDOT:PSS as a 2-phase material. Adapted from [41].

Stretchability

The stretchability of PEDOT:PSS in the intrinsic form is relatively low (<10%) [27, 28]. It is a semi-crystalline polymer in the solid state. Some research has been focused on improving the stretchability. There are two main approaches: adding a small-molecule plastizicer or embedding the conductive material in a soft polymer matrix. Both of these approaches aim at increasing the free volume between the coiled up chains of PEDOT and PSS [29]. Adding a plastizicer such as xylitol, glycerol or Triton X-100 can decrease the interaction between the chains of the polymers, which results in an increase in stretchability [28, 29]. Blending PEDOT:PSS with a polymer requires the latter to be water-soluble, which is a reason why PVA, Polyethylene Glycol (PEG) and Polyethylene Oxide (PEO) are among the most common additives.

There are two trade-offs to consider with these approaches. The conductivity will decrease with an addition of a secondary polymer, while adding a plastizicer can increase the conductivity [28]. This trade-off can be somewhat resolved by ionic-liquid doping, leaving the elasticity of the material unchanged while increasing the conductivity.

In one study, the effect on the elasticity of PEDOTS:PSS films by the addition of soft polymers was investigated. The aqueous PEDOT:PSS was blended with PEG, PEO and PVA of varying molecular weights. The blends were cast into 1 μm films and the films were subjected to uniaxial strain until breakage occurred. The results showed an increase in strain at breakage for all of the films, with PEO and PEG blends having an elongation of 25-40% and the PVA blend up to 50% elongation at breakage. Furthermore, the PEG/PEO films displayed a decrease in stress at elongation. However, at large fractions of PEG and PEO, the viscosity of the blend became too high to be processed in liquid form.

The effect of using Stretchability and Conductivity Enhancer (STEC) enhancers such as ionic-liquids in PEDOT:PSS films has also been investigated [31]. PEDOT films with different ionic-liquids were deposited on highly elastic substrates. The films were uniaxially strained and their conductivities were measured. The results showed that using a STEC enhancer in PEDOT films can substantially increase the conductivity while allowing for a high stretchability. The best results showed an increase in conductivity from 3100 S cm^{-1} at 0% strain to 4100 S cm^{-1} at 100% strain. The authors assign the partial resolve of the conductivity-stretchability trade-off to the morphology change in the material when adding STEC enhancers as described in Figure 2-14. The proposed explanation was that the STEC enhancers serve a dual purpose: an increase in volume of the PEDOT:PSS chains, while serving as a conductive element in the polymer matrix.

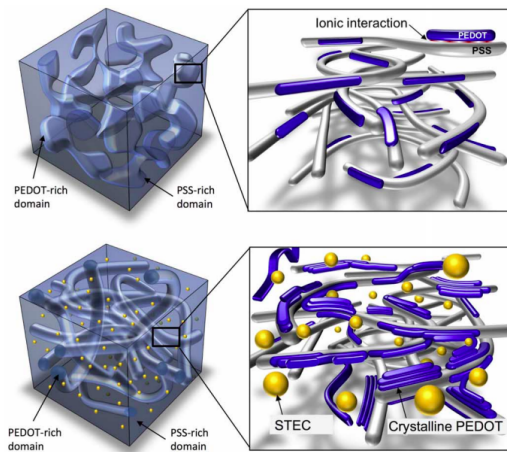


Figure 2-14: Morphology change when adding STEC enhancers to PEDOT:PSS. Figure courtesy [31, Fig. 1].

3 | Methodology

This chapter contains a detailed description of the methodology that was used to conduct the research. The main research methods are explained, as well as the strategy that was used to produce valid results. The reader can use this information to draw conclusions about the reliability of the experimental work.

3.1 Research strategies

In this thesis, an experimental research strategy was used. The strategy is based on varying background factors for the experiments and recording the outcome. Based on the observations, conclusions can be made regarding the impact of changing the factors. The project was focused on using DIW for energy storage devices and finding the optimal process settings for printing. Many different settings were tested in an attempt to fabricate the best possible devices and to avoid trade-offs. Formulation of the materials used for the experiments was also investigated using a similar approach. A variety of compositions were formulated and investigated quantitatively using the described methods.

3.2 Methods

This section covers the methods that were used for characterizing the performance of the fabricated MSCs.

Cyclic Voltammetry (CV)

A commonly used method for characterization of energy storage devices is Cyclic Voltammetry (CV). The method works by applying a potential to the device through a *potential window* at a linear voltage ramp. The current is measured as a function of the voltage and is presented in the form of a cyclic voltammogram [15]. The current in an ideal capacitor is described by the equation

$$I = C \times \frac{dV}{dt} \quad (3.1)$$

where C is the capacitance and dV/dt the time-derivative of the potential, also known as the scan rate. Thus the data in a CV measurement is scan

rate dependent. A low scan rate has the advantage of allowing time for the ions to diffuse further into the electrodes resulting in a higher capacitance, however measurements at low scan rates are more time-consuming. A CV-measurement is normally performed at several different scan rates for a more complete understanding of the device behavior. The potential window during CV depends on the specific electrolyte being used.

From the voltammogram, the capacitance of the device can be calculated using the equation

$$C_A = \frac{\int_0^{\Delta V} (I_C - I_D) dV}{2 \times \nu \times A \times \Delta V} \quad (3.2)$$

where I_C and I_D are the charge and discharge currents, ν is the scan rate of the measurement, A the device area and ΔV the potential window. The factor 2 in the denominator comes from the fact that the capacitive influence of both charging and discharging is included in the integration of an entire CV plot. Thus the plot is assumed to be symmetrical around the x-axis.

The characteristic voltammogram of an ideal EDLC is a nearly rectangular plot with instant current saturation upon applying a voltage as described in Figure 3-1 [15]. However, a deviation often occurs due to faradaic reactions and internal resistance in the electrodes and electrolyte of the cell. This is usually manifested by a more or less *lens-shaped* plot.

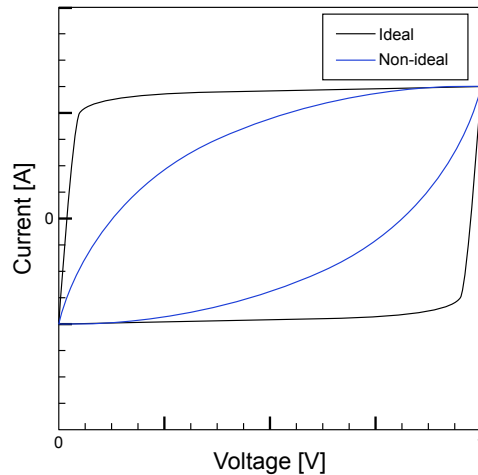


Figure 3-1: Typical appearance of a CV plot for an EDLC.

Galvanostatic Charge-Discharge (GCD)

An important aspect of energy storage devices is the charge-discharge cycle time. In Galvanostatic Charge-Discharge (GCD), the device is charged with a constant current until a voltage setpoint is reached and subsequently discharged. The time for the full charge-discharge cycle is recorded and plotted against the voltage. This can provide important information about the resistance and capacitance of the device [15].

The areal capacitance of an EDLC is proportional to the discharge time [12]. Equation 3.2 can be rewritten on the form

$$C_A = \frac{I}{A} \frac{dt}{dV} \quad (3.3)$$

where A is the active area of the device and dt/dV the inverse of the slope of the GCD plot. For an ideal device, the slope is linear. However, a non-linear behavior during GCD cycling can sometimes be detected. An increased self-discharge can also contribute to a deviation from linearity. This behavior is represented in Figure 3-2.

The IR-drop in the insert of Figure 3-2 is indicative of the resistance in the cell and can be used to calculate the series resistance [15] by dividing the voltage drop with the current inversion.

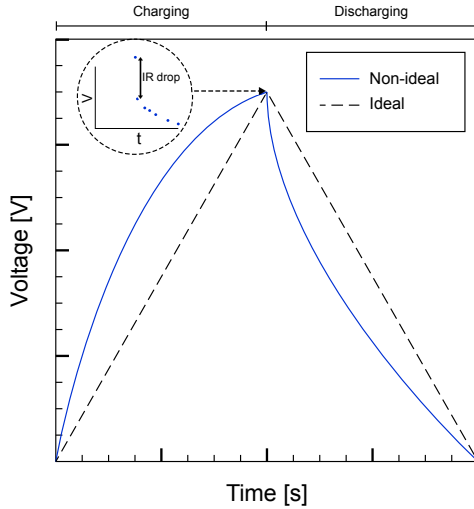


Figure 3-2: Typical appearance of a GCD plot for an EDLC.

Electrochemical Impedance Spectroscopy (EIS)

The resistance of a circuit is not only dependent on the magnitude of the current but also the phase. Electrical impedance is the equivalent of resistance for an alternating current. Electrochemical Impedance Spectroscopy (EIS) is a method for characterizing the impedance behaviour of an EDLC [12]. A low-voltage alternating current of a wide range of frequencies is applied to the device and the response is measured.

Figure 3-3 shows schematic results for a typical SC using EIS. The results are usually presented as both a *Nyquist plot* as shown in Figure 3-3a and a *Bode plot* as shown in Figure 3-3b. The Nyquist plot can be divided into two main sections. The semi-circle in Figure 3-3a represents the measurement at higher frequencies. The solution resistance R_s is the point where high-frequency processes are initiated. As the frequency decreases, mass transport processes such as diffusion become dominant [12, 15]. The impedance span between the two points is denoted the charge transfer resistance R_{ct} in the figure. As the imaginary part of the impedance Z_{im} reaches 0, the impedance is equivalent to that of a circuit exposed to a direct current. The corresponding Z_{Re} value is named the equivalent series resistance (ESR).

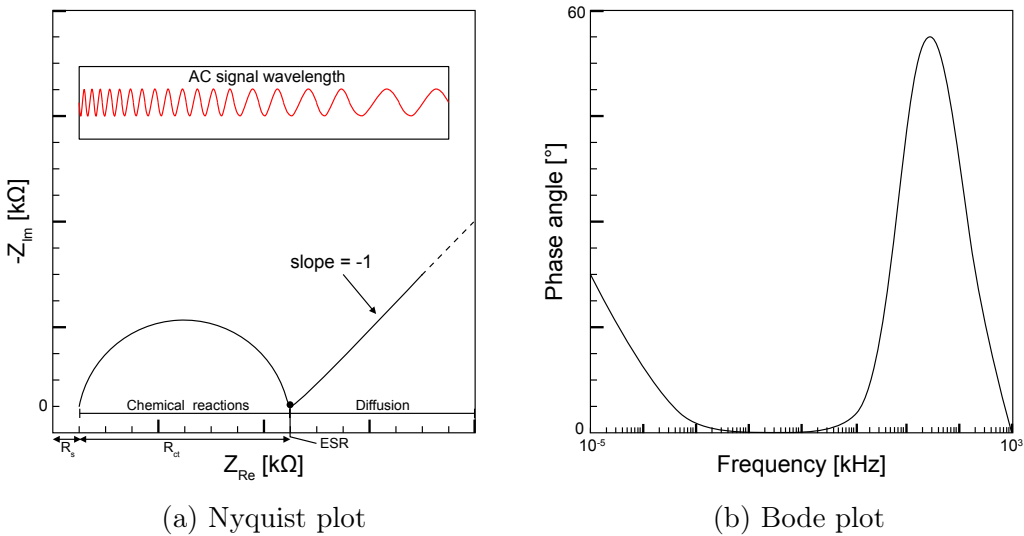


Figure 3-3: Schematic plots from EIS-measurements of a supercapacitor.

The Bode plot can be used as a way of characterizing the equivalent circuit of a system. The phase angle of the signal at varying frequencies is related to the types of components present in the circuit. The schematic plots from Figure 3-3 are typical for measurements of a so-called Randles circuit shown in Figure 3-4 [15]. The circuit consists of the following components

- R_S resistance in the bulk electrolyte
- R_{CT} resistance from charge-transfer processes
- C_{DL} double layer capacitance

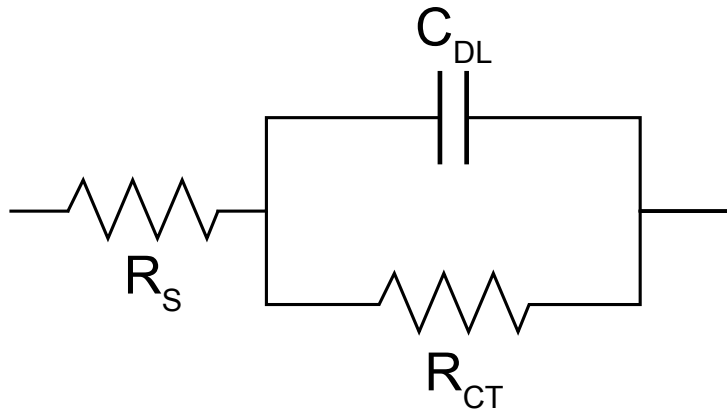


Figure 3-4: Randles equivalent electrical circuit.

3.3 Data collection and analysis

In this thesis, all of the data was collected through experiments. The experiments involved fabricating the devices using the printing methods described in Chapter 4. The devices were characterized using the standard characterization methods which are presented in Section 3.2. A Gamry Interface 1010E potentiostat was used for all data collection.

After collection of the data, it was converted to a format that could be analyzed using MATLAB which was the main tool for doing calculations, approximations and for presenting the data. Measurements from CV were used to approximate the capacitance of the devices, and this was compared to capacitance approximations using GCD. EIS was used to quantify the impedance behaviour of the devices.

3.4 Quality assurance

For the work in this thesis, a number of steps were taken to ensure a high quality of the research. The quality in this sense refers to the validity, repeatability, reproducibility and replicability.

- **Validity** To ensure that the results were devoid of artefacts, only commonly used methods were used for measurements. One example of such an artefact in this context could be to use a non-valid GCD plot to estimate the capacitance of a device. This was avoided by using several methods for capacitance approximations.

Another artefact to avoid was that the electrochemical performance of a device will appear to be higher if the electrolyte is not dry. Therefore, measurements were performed at regular intervals after applying the electrolyte. The devices were also re-measured after a long period of time. This helped to avoid drawing invalid conclusions about the lifetime of the devices.

- **Repeatability** The demand for repeatability of the results were met by fabricating at least two identical devices for each measurement. This translates to the same number of layers of material, same process settings and materials. The materials (inks and electrolytes) followed the same procedure for formulation and the process is disclosed in Chapter 4. Fabrication of each device was done in the same manner in terms of substrate cleaning, printer preparation. Furthermore, devices that were measured and compared were always fabricated from the same batch of materials.
- **Reproducibility** All of the process steps in terms of material formulation and printing are disclosed in Section 4. This ensures that the need for reproducibility is met. The steps taken for the experimental work in this thesis is made available in as great detail as possible. All of the produced results are presented to the reader. If a result is qualitative, it will be presented with a sufficient description together with images and figures to explain the observations.

4 | Experimental

4.1 Materials

The following section contains relevant information regarding the equipment, chemicals and materials that were used for the work in this thesis.

3D printing equipment

A FELIX Pro 2 3D printer was used for all of the printed devices in this work. Figure 4-1 shows the main parts of the printer. The printer was custom-ordered together with a Viscotec Vipro-HEAD3 that allows for extrusion of viscous 1-component fluids and pastes. The print head setup is shown in Figure 4-2. It is a rotary positive displacement pump using an endless piston principle to deliver a constant amount of material independent of changing parameters such as pressure or temperature [42]. This in turn means that it allows for dispensing of fluids without shear thickening, which is critical for the proposed printing technique. These properties makes it ideal for 3D printing of the materials proposed in this thesis. The Viscotec Vipro-HEAD3 was used together with Drifton precision stainless dispensing tips of inner diameter 0.25 mm and outer diameter 0.51 mm.

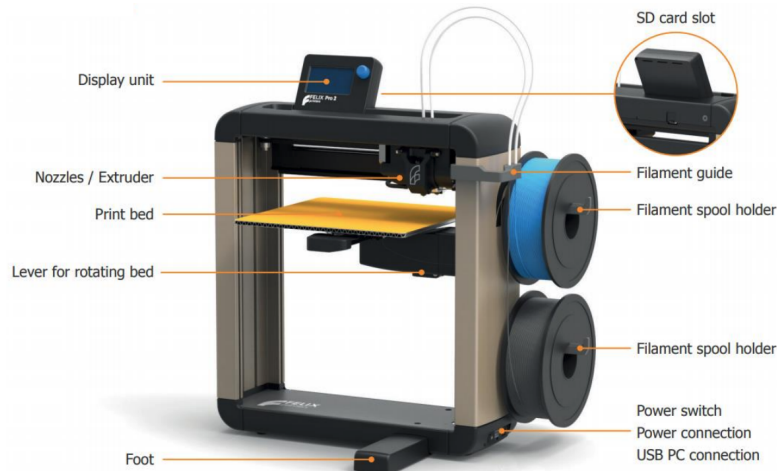


Figure 4-1: Main parts of the Felix Pro2 3D printer. Courtesy of [43].

There are several methods for using commercial 3D printers. Typically, a CAD drawing is generated using a commercially available software and is

subsequently imported into a *slicing software*. The slicing software converts the CAD design into a set of instructions that the printer executes. However, most commercial 3D printers are designed to print plastic materials and thus the slicing softwares optimize the print quality based on plastic materials. The slicing feature is however not optimal for printing viscous fluids. A different method for 3D printing is to use an interactive software such as Repetier Host, which the user can use to send instructions directly to the printer without the need for any additional slicing software. The user manually provides the printer with a set of x, y, z -coordinates and other necessary parameters. Using the described method facilitates the optimization for printing of non-standard materials.

Repetier Host was used for all prints presented in this report. There are many printing parameters that can be controlled in the Felix Pro 2 3D printer. The most influential parameters for the printed devices in this thesis are the feed rate (F), extrusion speed (E), bed temperature (T) and the nozzle height (Z). The following definition is used for the parameters:

- **Feedrate (F)**: speed of movement of the printhead (mm min^{-1})
- **Extrusion speed (E)**: amount of printed material (mm)
- **Bed temperature (T)**: temperature of the print bed ($^{\circ}\text{C}$)
- **Nozzle height (Z)**: distance from nozzle opening to bed surface (mm)

Table 4.1 summarizes how the parameters affect the final print. However, this list is not exhaustive as the parameters also have a synergistic effect. Likewise, the drawbacks of one parameter can sometimes be reduced by changing another. The method of finding proper settings involved a trial-and-error approach in which many different settings were tried and evaluated qualitatively.

Table 4.1: Printing parameters and their effects on print quality.

Parameter	Too high	Too low
F	Uneven line thickness	Low resolution
E	Low resolution	Nozzle clogging
T	Cracking	Poor wetting/adhesion
Z	Non-continuous printing	Smearing

Chemicals

In Table 4.2 the chemicals and compounds used for ink and electrolyte formulation are listed.

Table 4.2: Chemicals used for experiments.

Manufacturer	CAS	SKU	Name	Density [g L ⁻¹]
Sigma-Aldrich	25322-68-3	372838	PEO	N/A
Sigma-Aldrich	N/A	739332	PEDOT:PSS	11
Sigma-Aldrich	56-81-5	G9012	Glycerol	1250
Sigma-Aldrich	7664-38-2	40278	Phosphoric acid	1685
Sigma-Aldrich	7664-38-2	561223	PSSH	1110

Substrate materials

A Platilon® 4201AU extruded thermoplastic polyurethane (TPU) film from Epurex Films was used as substrate material for the printed devices. According to the manufacturer, the material has a tensile strain of 500% and a tensile stress of 65 MPa at break. These values are average values over a long period time and can vary with up to 30% between single productions. The manufacturer states that the material has a good adhesion to inks.

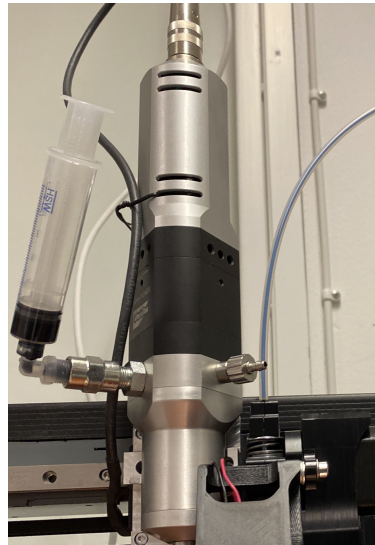


Figure 4-2: Viscotec Vipro-HEAD3 used for 3D printing.

4.2 Procedure

This section provides a detailed description of the methods and procedures that were used to carry out the experiments in the thesis. The section is divided into two parts. The first part describes the procedure for formulating the inks and electrolytes used for device fabrication. In the second part, the procedure for DIW and fabrication of the devices is described in detail.

Device fabrication

Ink formulation

An ink based on PEDOT:PSS for DIW of the device electrodes was formulated. Formulation of the ink was done by adding a plasticizer and a polymer matrix material in a beaker together with PEDOT:PSS and using mechanical stirring. The stirring speed for the inks varied between 60-100 RPM during the first 3 days, after which it was increased to 100-200 RPM. A slow stirring speed was necessary initially to maintain an effective mixing, as the viscous ink displayed sheer thickening properties. The proper mixing of the ink was facilitated by regularly using a VWR Labdancer S40 Mini Vortexer and an ultra sonic cleaner. The procedure was to use the Labdancer for 10 min while maintaining as constant a vortex as possible, which effectively ensured proper exchange of the material. Then the ink was transferred to the USC in which it was sonicated for 10 min. This step was performed 1-2 times.

Electrolyte formulation

Electrolytes used for the printed MSCs were formulated using the same plasticizer and polymer matrix material as the formulated ink. An ionic species was added to serve as the active material and the addition of H₂O facilitated the processing. Table 4.3 shows the main compositions of the electrolytes.

Table 4.3: Main compositions of the formulated electrolytes.

#	PSSH [mL]	H ₃ PO ₄ [mL]	H ₂ O [mL]
EL1	0	0.6	6
EL2	0.07	0	6
EL3	0.07	0.6	6

Direct Ink Writing procedure

After formulation, the ink was manually transferred to a syringe of size 10 mL which was connected to the Vipro-HEAD3 print head. The print head was left to purge the material until the material was being extruded without any interruptions. The TPU substrate was then thoroughly prepared. First, a cleanroom cloth prepared with Isopropyl Alcohol (IPA) was used to remove particles and organic residues on the substrate. The same treatment was performed on the print bed of the 3D printer. A handheld plasma gun was then scanned across the surface of the substrate to increase the hydrophilicity. The printbed temperature was set to 50 °C before printing, to promote adhesion between the printed material and the substrate. After heating, the substrate was placed on the print bed. A standard Scotch Tape was used to attach the substrate. One piece of tape was attached to each side of the substrate as shown in Figure 4-3a, and the substrate was stretched slightly to avoid wrinkles.

Printing was performed by running a GCode command script. The printing process was iterated many times to find the optimal settings. The printed structure consists of vertical and horizontal lines, so-called leader bars. The leader bars assure an even material flow through the print head, and the patterns can be used for resistance measurements without interfering with the device. Devices consisting of one layer of material were printed and immediately removed from the print bed. Devices consisting of several layers of material were left to dry as little as possible between subsequent layers in order to improve adhesion and avoid delamination.

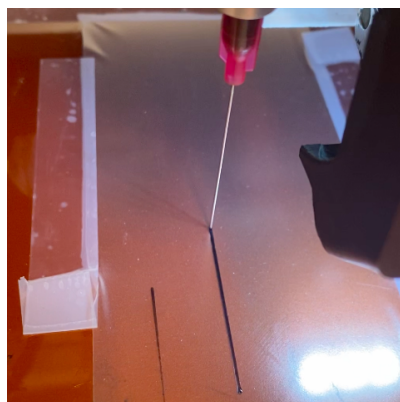
The two main background factors of interest were the effect of the number of passes of the printer and the electrolyte composition. The devices were fabricated with a varying number of layers using the same electrolyte, and with constant electrode layers but using different electrolytes. All of the measured devices are summarized in Table 4.4.

Table 4.4: Overview of the fabricated devices used for measurements.

Name	No. layers	Electrolyte	No. fabricated devices
1L_EL1	1	EL1	2
2L_EL1	2	EL1	2
4L_EL1	4	EL1	1
2L_EL1	2	EL2	2
2L_EL1	2	EL3	2

Electrolyte and probe contact application

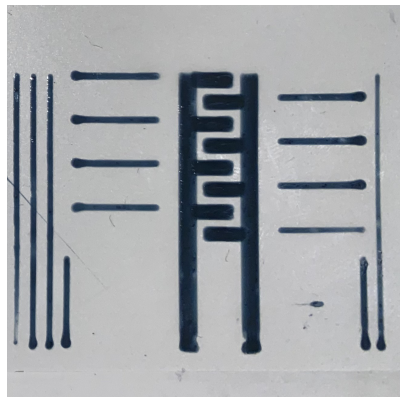
Contact pads for probing the devices were applied. A 5 mm × 5 mm copper tape was attached to the legs of the device. A small quantity of silver paste was used to form an electrical connection between the copper tape and the device. Electrolyte was applied to the printed devices by pipetting 300 µL of electrolyte in the center of the interdigitated structure. As the viscosity of the electrolyte prevented it from forming an even layer across the devices, a plastic pipett was used to spread the electrolyte evenly. After application, the device was left to dry in a fume hood at room temperature for. Drying time of electrolyte for initial tests was 6 h, and for the subsequent devices 24 hours.



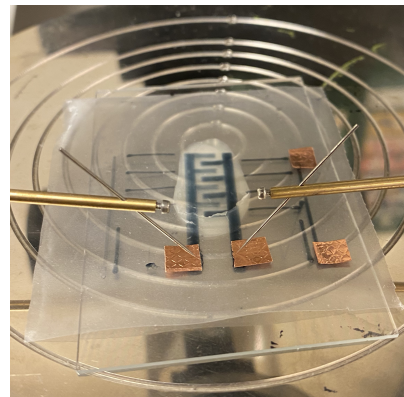
(a) 3D printing process



(b) Stretched pattern



(c) Printed pattern



(d) Measurement setup

Figure 4-3: Experimental process of fabrication and measurement.

4.3 Issues

Ink and electrolyte formulation

Material homogeneity

The main issue with formulating the ink and electrolyte materials was finding a procedure for the proper mixing of the constituents. PEO is water-soluble, however the dissolution of PEO in powder form is a slow process which requires a combination of mechanical stirring and sonication. Stirring allows for the concentration gradients within the material to be removed while sonication facilitates the separation of larger PEO agglomerates in the liquid. The proper mixing of the materials was qualitatively inspected. Improper mixing leads to a material which is very viscous and acts more as a gel than a liquid. On average, the formulation of a properly mixed ink and electrolyte was a process which required 4-5 days.

Ink lifetime

Another concern with the formulated ink was that it appeared to have a limitation on how long it could remain inside the printhead without becoming difficult to process. In general, the ink printability was very high when the ink was recently added to the printhead. With time, lumps of material would appear and the printability diminished. This process was qualitatively estimated to be 6-8 hours. This required devices from the same batch of material to be printed in the same day. It also set limitations on the scope of the thesis, as printing one batch of devices could take as much as 2 working weeks, including formulation, printing, cleaning of the printhead and device preparation with electrolyte and probe contacts.

3D printing

Delamination

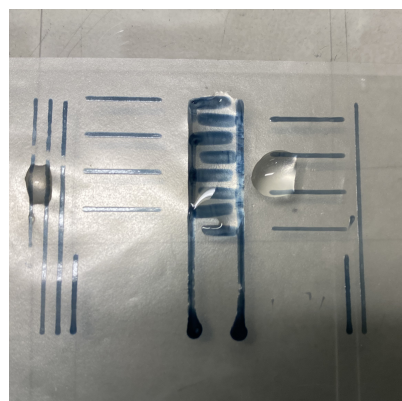
The major issue with the 3D printing part of the work was that the material had a tendency to delaminate, either from the substrate or from previous electrode layers. The issue of delamination from the TPU substrate was resolved by proper preparation of the substrate using IPA and a thorough preparation with plasma. However, delamination between subsequent electrode layers was not completely resolved. The issue appeared when the electrolyte was applied, upon which some layers would lift off and move from their original positions.

Several devices were discarded due to the electrodes coming in contact as a result from this issue.

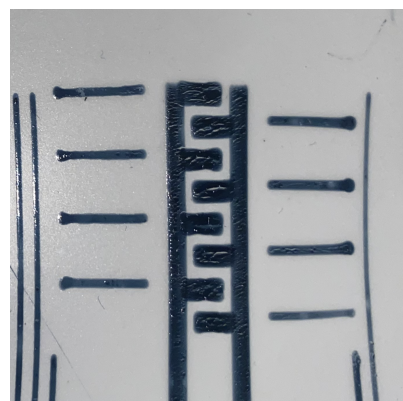
The issue was partially resolved by experimenting with the print settings. It was apparent that minimizing the time for drying between subsequent layer had an impact on this issue. Initially, a drying time of 10 was allowed between subsequent layers. At this drying time, delamination could be seen visually in roughly 50% of the devices. However, when printing the layers in as quick a succession as possible, the issue only appeared sporadically. The main method to circumvent this issue was to reduce the drying time, and also to print more devices than intended to measure.

Cracking

Cracking of the electrode material became apparent when stretching the electrodes to large strains. It was most severe for prints using many (4-8) stacked layers of material. When printing 1 layer of material, cracking was noted but less frequently. It was however apparent that the processing temperature was of important. Patterns with lines of length 2 cm and 2, 4 and 8 layers were printed to investigate the effect. When printing with a print bed temperature of 55 °C and treatment on a hotplate for 1 h, severe cracking was seen when straining the material. However, reducing the print bed temperature to 40 °C and no post-treatment at elevated temperature significantly reduced the amount of cracking. Notably, 1 layer of material could be printed with the latter settings and strained until the substrate ruptured without showing any evidence of cracking.



(a) Delamination



(b) Crack formation

Figure 4-4: Common issues associated with the 3D printing process.

Stretchability test

To test the stretchability of the PEDOT:PSS ink, U-shape patterns were printed. The printed pattern is displayed in Figure 4-5. Figure 4-5a shows the designed pattern and Figure 4-5b a printed sample. Samples of 2, 4 and 8 layers of material were printed to study the effect of adding more layers on the resistance and the stretchability of the ink.

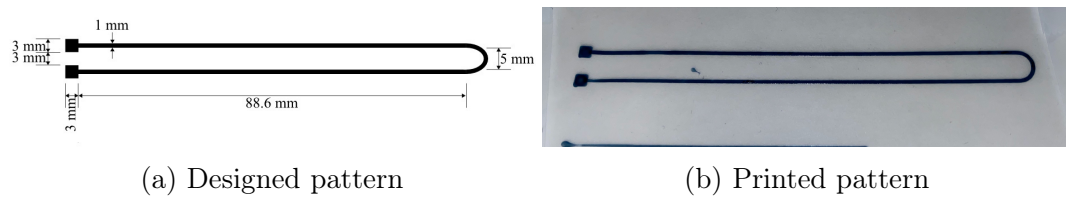


Figure 4-5: U-shape patterns for ink stretchability measurements.

The stretchability of the ink was investigated by applying a strain in the x-direction while simultaneously recording the resistance. Measurements were performed in Tampere University, Finland. The test setup is shown in Figure 4-6. The applied strain can be defined using the equation

$$\varepsilon(\%) = \frac{\Delta L}{L_0} \times 100 \quad (4.1)$$

L_0 denotes the length between the sample holders before the strain was applied and is schematically shown in Figure 4-6. The strain at the point where the normalized resistance has increased by more than 100% was defined as the stretchability. For all measurements, the value of L_0 was 50 mm.

The stretchability of the electrolyte was investigated qualitatively. 500 μL of each of the formulated electrolytes was pipetted on to the TPU substrate and left to dry in the fume hood. After drying the electrolyte for 24 h, the substrate was strained to roughly 50% and a comparison was made between the materials.



Figure 4-6: Test setup used for stretchability tests of the formulated ink. The measurements were performed at Tampere University (TAU). The value of L_0 was 50 mm

5 | Results

5.1 Electrochemical characterization

This chapter contains the results from electrochemical characterization of the fabricated devices. CV-measurements were performed to quantify the areal capacitance of the devices. A detailed description of the capacitance calculation is also provided. To see the influence of parameters such as material layers and electrolyte, the results of CV and EIS-measurements have been divided according to the specific parameters of the device. The device that displayed the most promising results from CV-measurements was chosen for GCD

Cyclic Voltammetry

The fabricated devices listed in Table 4.4 were measured using CV. For each measurement, 3 scans were made. The third scan was selected for evaluation. The devices were scanned using scan rates of 5 mV s^{-1} - 5000 mV s^{-1} . Scan rates above 100 mV s^{-1} were excluded from the results section. First, the 4-layer device with EL1 was measured. The results showed signs of the electrolyte not being dry (e.g. non-symmetric CV-plot). This effect was thus investigated before measuring the other devices. The electrolyte drying time for the 4-layer device was 6 h before the initial measurement. For the other devices, the drying time for the electrolyte was 24 h. Results from the CV-measurements are presented in the following subsections.

1 layer electrodes with EL1

A device with 1 layer of electrode material were fabricated and measured using CV. Figure 5-1 shows the results from one of the measurements. At lower scan rates, the current is increasing relatively slowly, whereas at higher scan rates the CV-curve is lens-shaped and displays no current saturation behavior.

The device had an average cell capacitance ranging from $290 \mu\text{F cm}^{-2}$ at a scan rate of 5 mV s^{-1} to $24 \mu\text{F cm}^{-2}$ at a scan rate of 100 mV s^{-1} . The deviation from the average capacitance at the respective scan rates was $\pm 6\%$ and $\pm 3\%$.

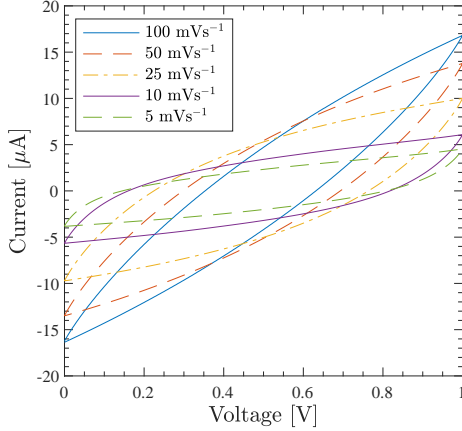


Figure 5-1: CV measurements of 1-layer electrodes with EL1.

2 layer electrodes with EL1

The results from CV-measurements presented in Figure 5-2 are from a device with twice the number of electrode layers as in Figure 5-1. Comparing the two figures, it can be seen that the area under the voltammogram has increased. The characteristic lens-shape appearance of the CV-curve is apparent, especially at higher scan rates.

As for the previous device, the capacitance was approximated. At the lowest and highest scan rates, the average capacitance of the two devices was $434 \mu\text{F cm}^{-2}$ at a scan rate of 5 mV s^{-1} and $20 \mu\text{F cm}^{-2}$ at a scan rate of 100 mV s^{-1} with deviations of approximately $\pm 2\%$ at both scan rates.

Notably, when the number of electrode layers was increased from 1 to 2 using the same electrolyte (EL1), the average specific capacitance increased at the lowest scan rate with approximately 50%. At scan rate 25 mV s^{-1} , there was a slight decrease of capacitance when increasing the number of electrode material layers. The decrease at the highest scan rate was approximately 20%. This effect can be seen qualitatively with the area under the curve for the 100 mV s^{-1} appearing smaller in Figure 5-2 than in Figure 5-1.

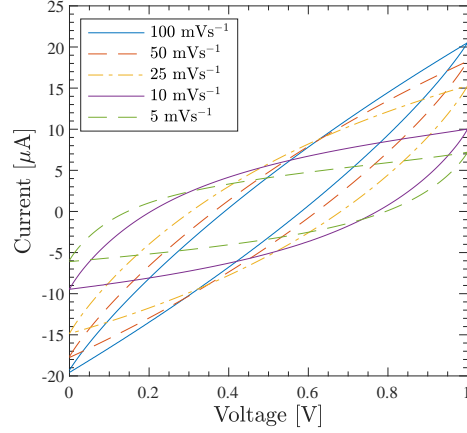


Figure 5-2: CV measurements of 2-layer electrodes with EL1.

4 layer electrodes with EL1

In figure 5-3, the results from CV-measurements of one device with 4 layers of electrode material and electrolyte EL1 are presented. Comparing with the 1-layer and 2-layer electrodes with the same electrolyte, the maximum current is substantially higher. It can be seen that the shape of the CV-curves at the lower scan rates are not as symmetric as in the previous figures. The approximated capacitance at the scan rates 5 mVs^{-1} and 100 mVs^{-1} were 3.2 mF cm^{-2} and $252 \mu\text{F cm}^{-2}$ respectively.

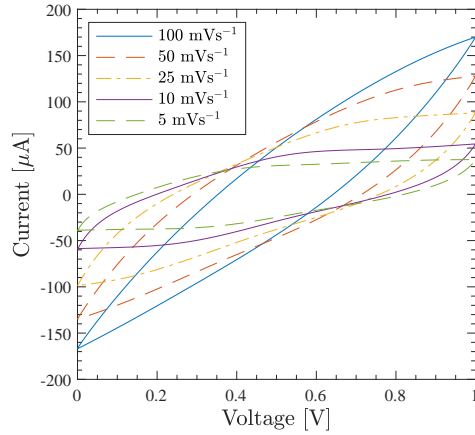


Figure 5-3: CV measurements of 4-layer electrodes with EL1.

2 layer electrodes with EL2

The results from using electrolyte EL1 showed that there was an increase in capacitance at low scan rates with an increase in the number of electrode layers while there was a decrease at higher scan rates. 4 layers of electrode material was also investigated. However, from a processing point of view, more electrode layers requires more time for drying. Delamination of subsequent layers was also an issue. For these reasons, 2 layers was chosen for investigating the performance of electrolytes EL2 and EL3. Electrodes with 2 layers of material were printed and EL2 was applied. The results from CV-measurements are shown in Figure 5-4. The performance is similar to that of the 2 layer electrode with EL1. The capacitance approximation showed an average capacitance of $450 \mu\text{F cm}^{-2}$ at 5 mVs^{-1} and $14.6 \mu\text{F cm}^{-2}$ at 100 mVs^{-1} . However, it can be seen from Figure 5-4 that the results from measurements of the two devices are very different. Figure 5-4a shows a lens-shaped CV-curve with a low maximum current, whereas Figure 5-4b has significantly higher maximum current. For these devices, the deviation from the average is thus large.

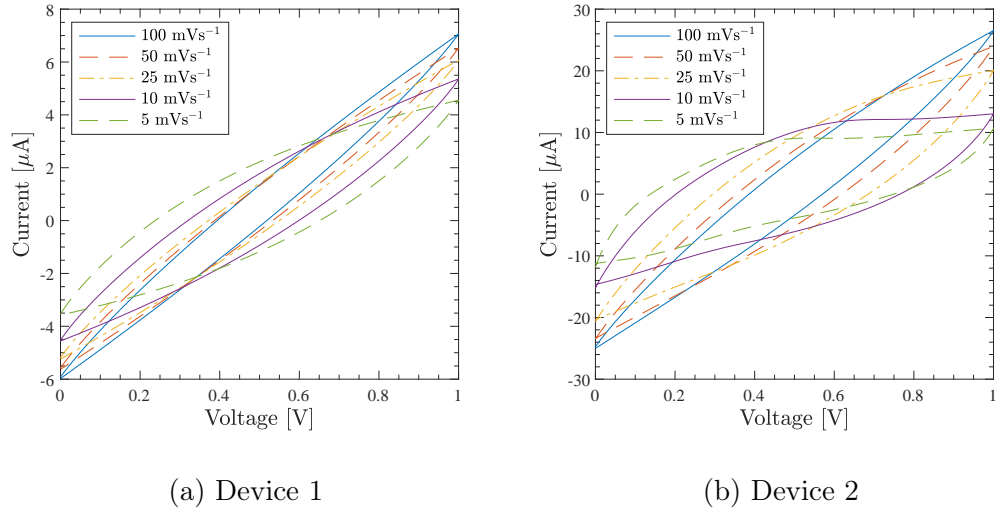


Figure 5-4: CV measurements of 2-layer electrodes with EL2.

2 layer electrodes with EL3

2 layer electrodes were also used together with electrolyte EL3 and the results from CV-measurements are presented in Figure 5-5. The results are similar to those in Figure 5-4b for electrolyte EL2. At the lowest scan rate, the current

reaches a saturation at roughly 0.4 V. The average capacitance values were $740 \mu\text{F cm}^{-2}$ and $52 \mu\text{F cm}^{-2}$ at the lowest and highest scan rates respectively.

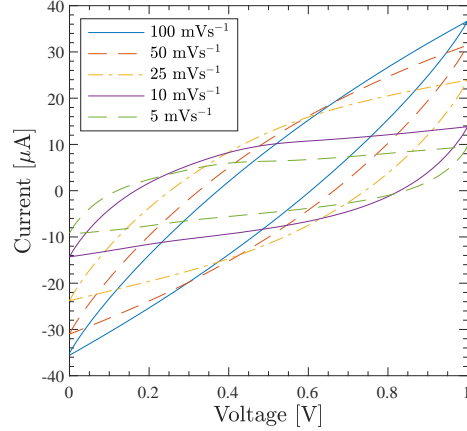


Figure 5-5: CV measurements of 2-layer electrodes with EL3.

Capacitance approximation using CV

The measurements from cyclic voltammetry were used to approximate the capacitance of the printed devices according to equation 2.1. The integration was done using a MATLAB script that analyzes the data obtained from measurements. By using a trapezoidal integration method, the integral is approximated. Figure 5-6 visualizes this method. The upper bounding area is in essence the sum of the blue and orange areas. The orange area is subtracted from the total which leaves the blue area as the integral.

In Figure 5-7, the results from CV-measurements of the devices are summarized. Figure 5-7a shows the approximated capacitance values of the different devices as a function of the scan rate. The values were calculated using Equation 3.2 with a value of the devices active area of 1.30 cm^2 . All displayed values of capacitance with error bars are average values from measurements on two separate devices that were fabricated in the same manner.

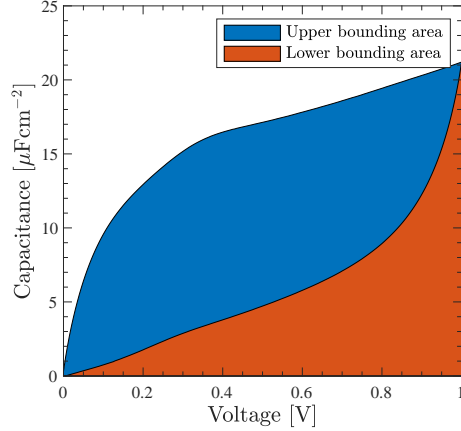


Figure 5-6: MATLAB integration of CV-curve.

Figure 5-7b shows the approximated areal capacitance of 2-layer electrodes with the three different electrolytes. The results are shown as the capacitance as a function of the acid content in the electrolyte. The values in the figure are given for the CV-measurement at scan rate 5 mV s^{-1} .

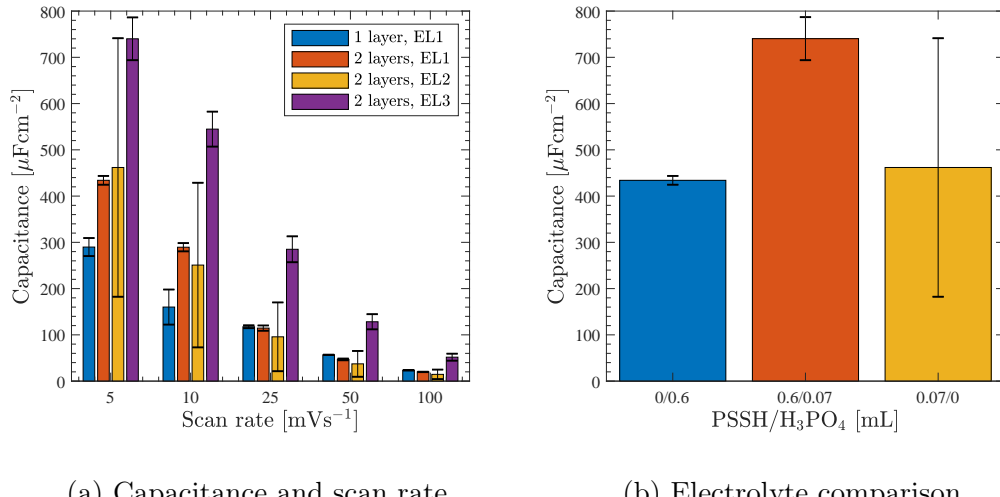


Figure 5-7: Calculations of the areal capacitance of the printed devices.

Cycling stability

The 4-layer device that was used in CV-measurements was also used for further investigations. These tests were mainly performed to investigate if the device is affected by cycling. Another point of interest was to find out if the effects of the electrolyte not being dry can be seen in the CV-measurements.

The device was cycled 350 times at a scan rate of 25 mV s^{-1} . The total cycle time was $\sim 8 \text{ h}$. Figure 5-8 shows the dependence on cycling of the CV-behaviour of the device. It can be seen in the figure that the initial maximum current at the scan rate is lower than that in Figure 5-3. This could be due to the electrolyte drying between the two measurements, which were performed roughly 2 apart. During cycling, there is a clear decrease of the area under the voltammogram. After 140 cycles, the capacitance decreased by approximately 40% from $840 \mu\text{F cm}^{-2}$ to $504 \mu\text{F cm}^{-2}$. After another 210 cycles, the capacitance decreased by another 35% to $328 \mu\text{F cm}^{-2}$.

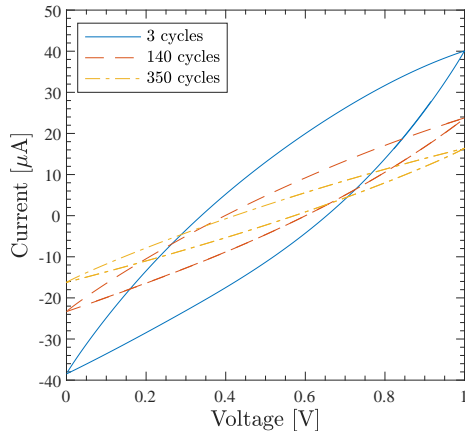


Figure 5-8: CV-measurement over a large number of cycles.

Device lifetime

To investigate whether the device lifetime, the 2-layer electrode with EL3 was re-measured 6 weeks after the initial measurements. This was also done to confirm that the initial CV-measurements were not affected by wet electrolyte. The specific device was chosen since it proved to have the highest measured capacitance of the 2-layer devices, and was thus of most interest to investigate further.

Figure 5-9 shows the initial measurement together with the second measurement of the device 6 weeks after. The results reveal that the maximum current decreased by approximately 15% from being stored. The capacitance of the device also decreased by roughly the same percentage at both high and low scan rates.

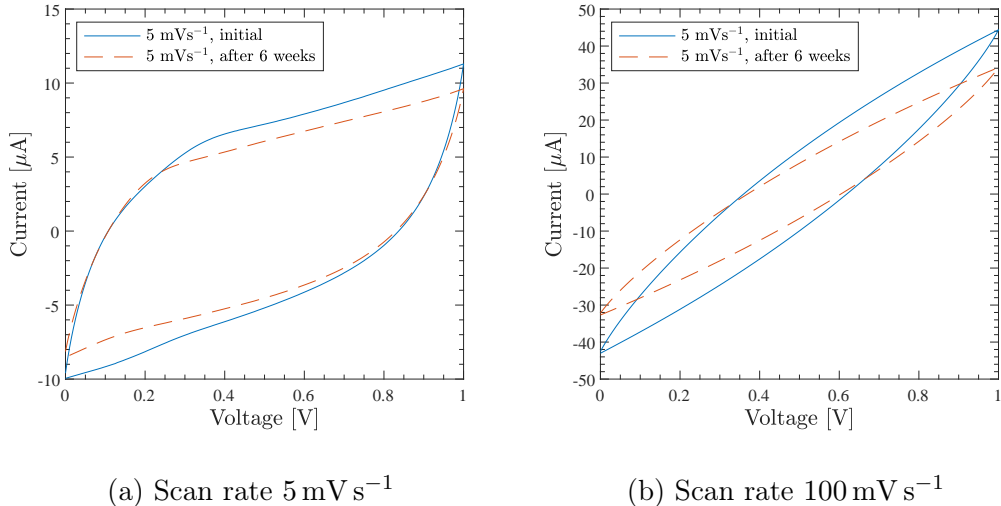


Figure 5-9: Comparison of CV-measurements over time.

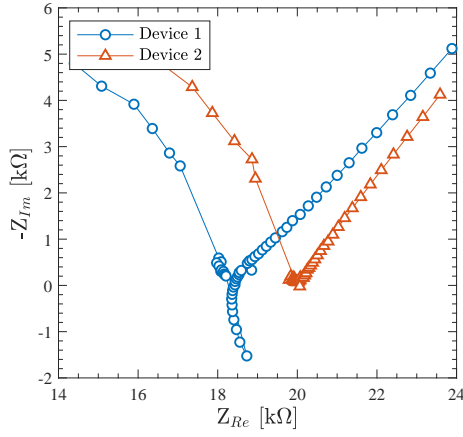
Electrochemical Impedance Spectroscopy

The devices were measured using EIS. The measurements were performed prior to the CV-measurements and are presented as Nyquist plots and Bode plots for each device.

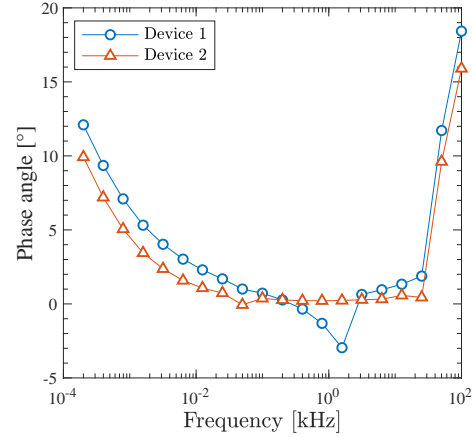
1 layer electrodes with EL1

The EIS measurements from the 1-layer electrode devices with electrolyte EL1 are presented in Figure 5-10. In Figure 5-10a the Nyquist plot of the devices is shown. Both devices have a similar response to the applied signal. One difference is that the device 1 has a positive imaginary part of the impedance around the ESR point. The second device that was measured shows signs of the characteristic ideal capacitor behavior, with an ESR of approximately $20 \text{ k}\Omega$.

The Bode plots in Figure 5-10b show a similar response for both devices.



(a) Nyquist plot

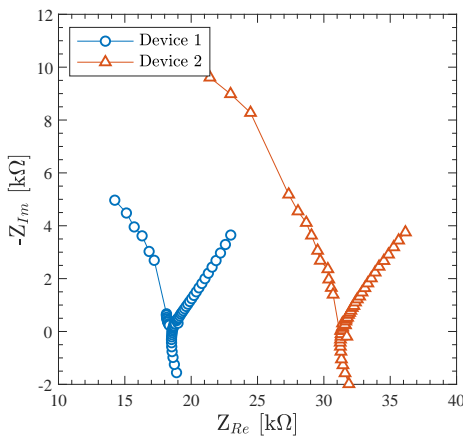


(b) Bode plot

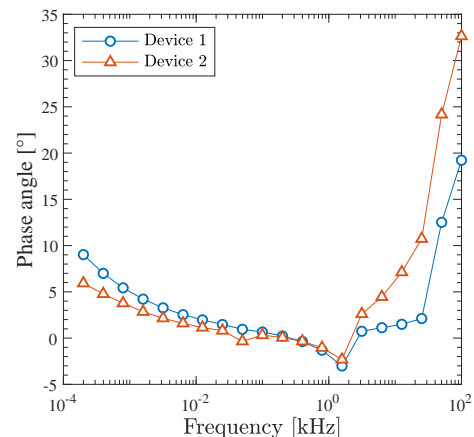
Figure 5-10: EIS measurements of 1-layer electrodes with EL1.

2 layer electrodes with EL1

In Figure 5-11 the results from EIS-measurements on the 2-layer electrode device with electrolyte EL1. The behavior of the devices in Figure 5-11a is similar that of the 1-layer electrode device. The positive Z''_{Im} values around the ESR point are present for both devices. The ESR values are in a range of 19-32 k Ω .



(a) Nyquist plot



(b) Bode plot

Figure 5-11: EIS-measurements of 2-layer electrodes with EL1.

4 layer electrodes with EL1

The 4-layer electrode device was measured using EIS and the results are presented in Figure 5-12. In the Nyquist plot in Figure 5-12a, the behaviour is similar to that of the 1-layer and 2-layer electrode devices. The ESR is comparable to the devices using the same electrolyte, at an approximate value of $37 \text{ k}\Omega$.

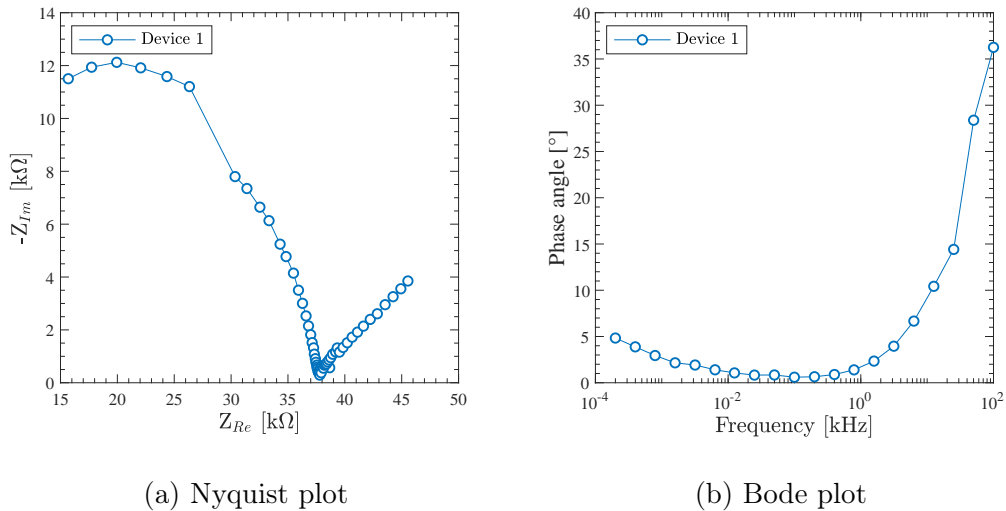
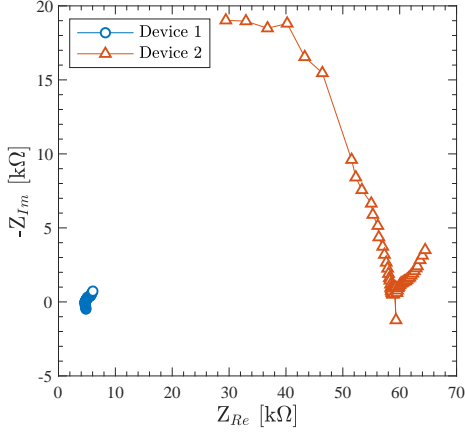


Figure 5-12: EIS-measurements of 4-layer electrodes with EL1.

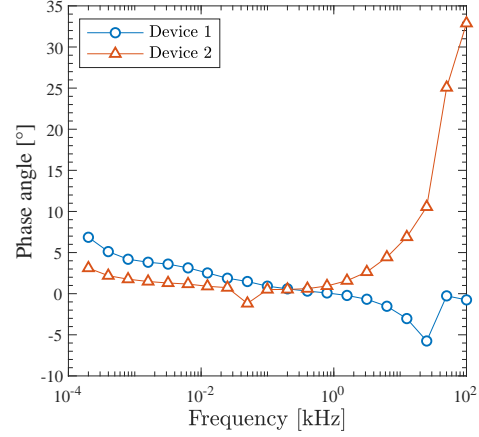
2 layer electrodes with EL2

The 2-layer electrode devices using electrolyte EL2 have some major differences from the devices using electrolyte EL1. In Figure 5-13a, measurements from both of the fabricated are presented. There is an apparent discrepancy between the two devices. Device 1 shows signs of not being measured properly, as there were only a few data points available from the measurement. Device 2 was similar in appearance from the devices using electrolyte EL1, however the ESR is significantly higher at an approximate value of $59 \text{ k}\Omega$.

Figure 5-13b also reveals some difference between the two devices. The phase angle is low for device 2 below frequencies of approximately 1 kHz. At higher frequencies, the phase angle of device 2 rapidly increases while this is not the case for device 1.



(a) Nyquist plot

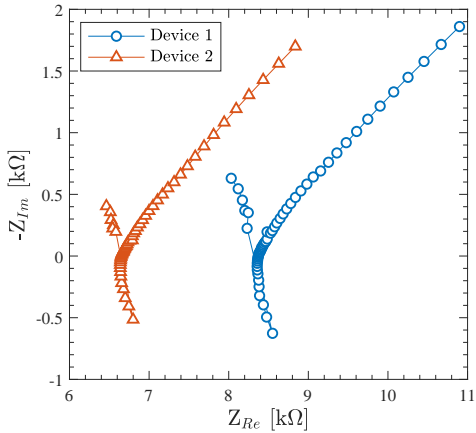


(b) Bode plot

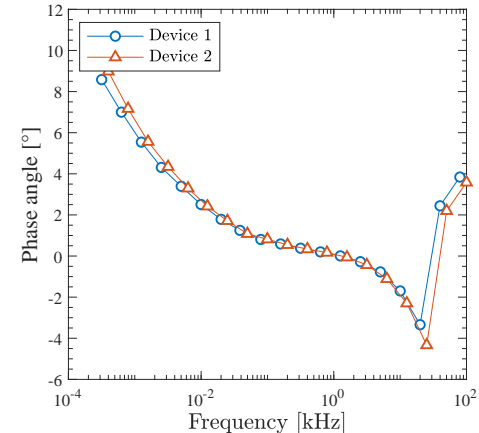
Figure 5-13: EIS measurements of 2-layer electrodes with EL2.

2 layer electrodes with EL3

Measurements from the 2-layer electrodes with electrolyte EL3 are presented in Figure 5-14. The ESR in Figure 5-14a is significantly lower than that of any of the other measured devices. The lowest recorded value is for device 2 at approximately 7 kΩ. In Figure 5-14b, there is no rapid increase in phase angle when moving to higher frequencies.



(a) Nyquist plot



(b) Bode plot

Figure 5-14: EIS measurements of 2-layer electrodes with EL3.

The average values of the ESR recorded for the fabricated devices is summarized in Figure 5-15.

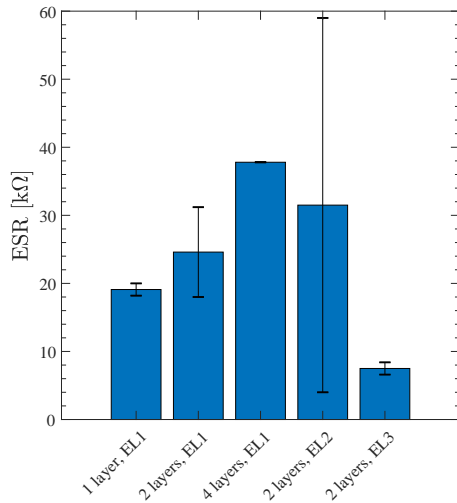


Figure 5-15: Summary of the ESR recorded for the measured devices.

Galvanostatic Charge-Discharge

The 2-layer electrode device with electrolyte EL3 was chosen for measurements using GCD. This specific device was chosen because it displayed the highest measured values of capacitance in CV-measurements, as well as the least ESR from EIS-measurements. The device was cycled at a charging current of approximately $7.7 \mu\text{A cm}^{-2}$ for 6 cycles. Measurements were performed 6 weeks after the initial CV-measurements. Figure 5-16a shows the results. The total cycle time is roughly 175 s. There is a distinct IR-drop of approximately 0.233 V present. The slope of the curve during charging and discharging shows signs of non-linearity during the charging cycle.

The device was also tested using higher currents of $15.4 \mu\text{A cm}^{-2}$ and $23.1 \mu\text{A cm}^{-2}$. Figure 5-16a shows the measurements at the different currents. At the highest charging/discharging, the cycle time is approximately 40 s. However, at this current, the IR-drop increased to nearly 0.8 V.

Capacitance approximation using GCD

A capacitance approximation was made using the data from GCD-measurements and Equation 3.3. The slope of the curve measured at the lowest current shows

signs of non-linearity and was roughly approximated. The inverse slope was suggested to be 123 s V^{-1} using the data points at 0.4 V and at 1.0 V. Using the active electrode area of 1.30 cm^2 , the capacitance is estimated to be $952 \mu\text{F cm}^{-2}$.

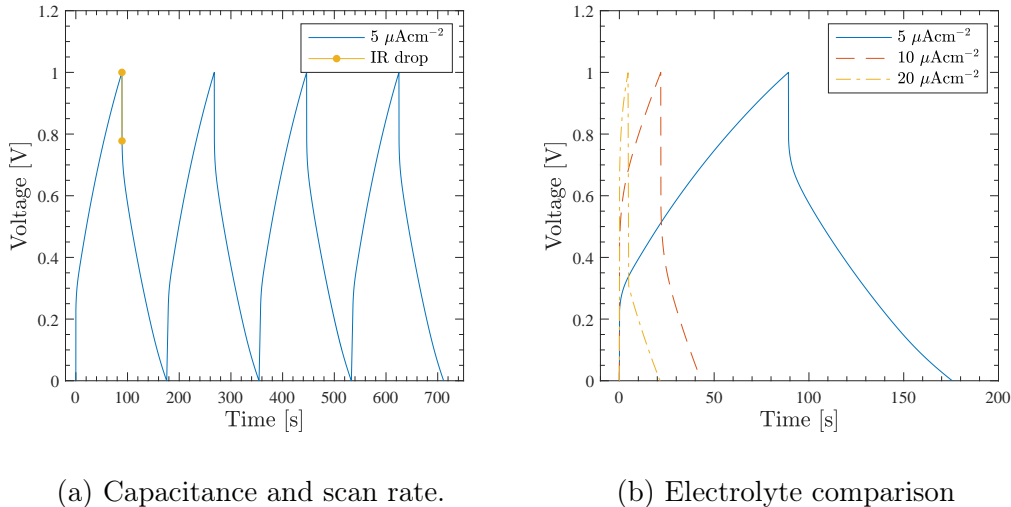


Figure 5-16: Calculations of the areal capacitance of the printed devices.

Stretchability test

Figure 5-17 shows the results from the ink stretchability tests performed at Tampere University, Finland. In Figure 5-17a, the results from two samples of patterns with 2 layers of material are presented. Both samples appear to have a similar response to the applied strain. At 80% elongation, the resistance is close to the initial value. At strains above 80%, there is a rapid increase in resistance. The average resistance value for the initial unstrained samples was $7.8 \text{ k}\Omega$.

The results are similar to those of the samples with 4 layers of material in Figure 5-17b. Two of the samples withstood a strain of 50%, after which the conductance rapidly disappeared. One sample tolerated a strain of 80% before rapidly increasing. The average initial resistance for that sample was $6.1 \text{ k}\Omega$. The results from the sample with 8 layers of material shown in Figure 5-17c reveals a stretchability of 50% and an average initial resistance of $2.2 \text{ k}\Omega$.

The stretchability of the three formulated electrolytes was investigated qualitatively by letting an equal amount of each electrolyte dry for 24 h on

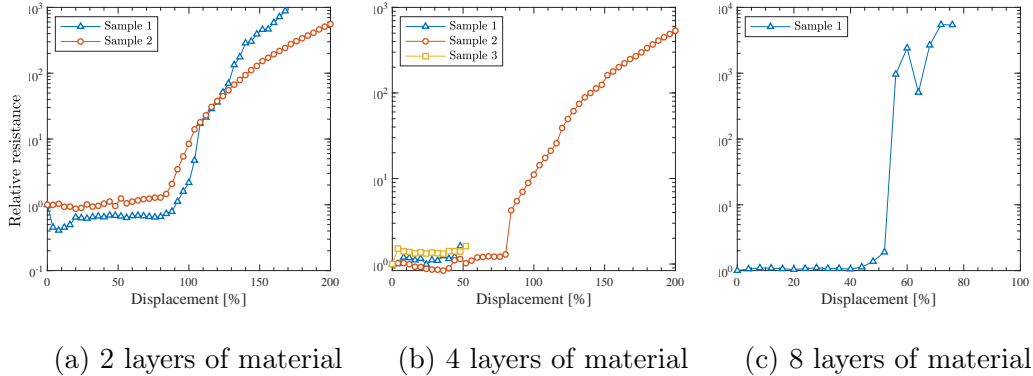


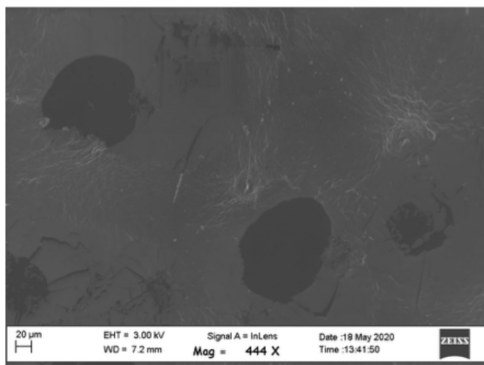
Figure 5-17: Results from stretchability tests performed at Tampere University (TAU). The figures show the normalized resistance as a uniaxial strain is applied.

the stretchable TPU substrate. The substrate was uniaxially strained to approximately 50%. A visual inspection suggests that electrolyte EL1 displayed the least strain tolerance with cracks forming on the entire electrolyte area. Electrolyte EL2 also has crack formation, but less pronounced and primarily around the edges, while electrolyte EL3 displays the highest strain tolerance with no visual cracks forming.

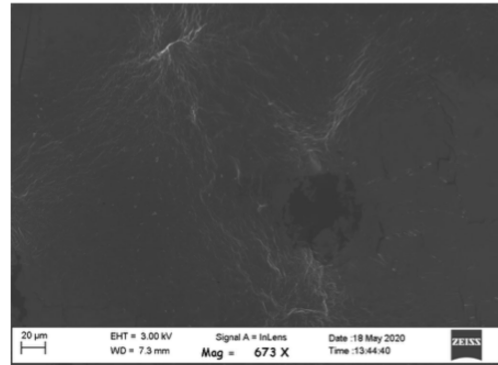
5.2 Materials characterization

Scanning Electron Microscopy

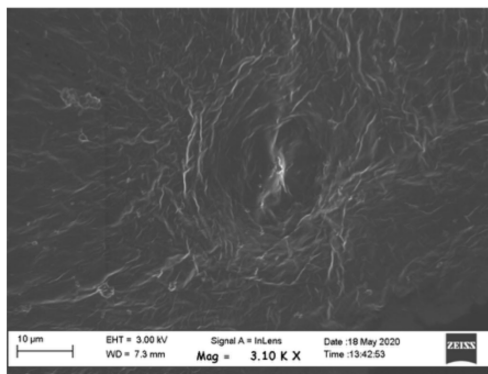
The formulated electrode material was printed on the stretchable TPU substrate and was examined using Scanning Electron Microscopy (SEM). Figure 5-18 shows the morphology of the PEDOT:PSS electrode at different magnifications. In Figure 5-18a, smooth areas coupled with clusters in brighter color can be seen. The dark spots are due to residual solvent from fabrication. Figure 5-18b shows two of the clusters forming a connection. The clusters in the figure are magnified and shown in detail in Figures 5-18c and 5-18d. At larger magnification, the microstructure of the material appears to be wrinkled surrounding a central point.



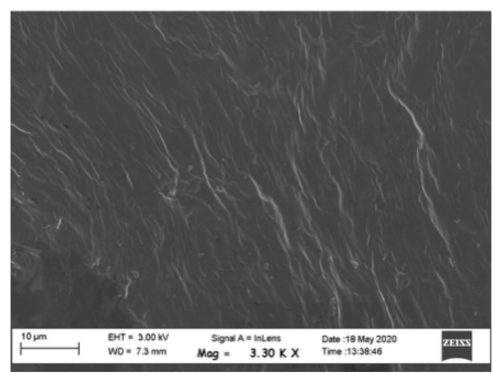
(a) Morphology of electrode material



(b) Two joined material clusters



(c) Material forming a cluster



(d) Wrinkled electrode microstructure

Figure 5-18: Images from SEM showing the morphology of the PEDOT:PSS electrode material fabricated by DIW.

6 | Conclusions

In this thesis, DIW of stretchable SCs was investigated. The purpose was to develop intrinsically stretchable materials and a simple DIW process for a stretchable SC. A PEDOT:PSS electrode material was developed. Three different electrolytes were formulated based on PSSH and H₃PO₄. Various experiments were performed on the fabricated devices to investigate and optimize the electrochemical properties. The stretchability of the ink was also investigated.

Results showed an increase in capacitance when increasing the number of electrode layers from 1 to 2 by approximately 50%. This increase in capacitance is likely due to the increase in electrode thickness. The best device displayed an areal capacitance of approximately 740 F cm⁻². The order of magnitude was confirmed using GCD. EIS revealed the lowest ESR of approximately 7 kΩ. Using an electrolyte with both PSSH and H₃PO₄ increased the areal capacitance by approximately 50% compared to devices with electrolyte consisting of either ionic species. The process responsible for the synergistic effect of the ionic species requires further explanation. Stretchability measurements showed a maximum stretchability of 80% for the developed ink.

In conclusion, this thesis has shown the feasibility of using a simple DIW method using commercially available materials to fabricate intrinsically stretchable materials for SCs. Figure 6-1 shows reported values from other studies in which similar devices were fabricated. Although the devices in this work show a lower areal capacitance, the other studies used either high-performance materials or complex fabrication techniques. Comparing this work to InkJet printed devices already shows promising results at low scan rates.

6.1 Outlook

Future development of intrinsically stretchable electrode materials should focus on incorporating materials such as graphene, MXene or silver nanowires into the ink to increase the conductivity. Another contribution would be to examine the printed devices using SEM and ellipsometry, to study the morphology and to characterize the power/energy density of the devices. Furthermore, this thesis studied the stretchability of the developed materials separately. However, the work did not include measurements of the fabricated devices while under strain. In order to compare the stretchability of the device with reported values, future work should be focused on fabricating the devices and

doing similar measurements while applying a uniaxial strain.

Although the main limitation of DIW is the resolution, this could be overcome by combining the proposed technique with other fabrication methods. One example of this is to use DIW to print highly uniform, strongly adhesive layers of material and to use LASER scribing to define high resolution patterns.

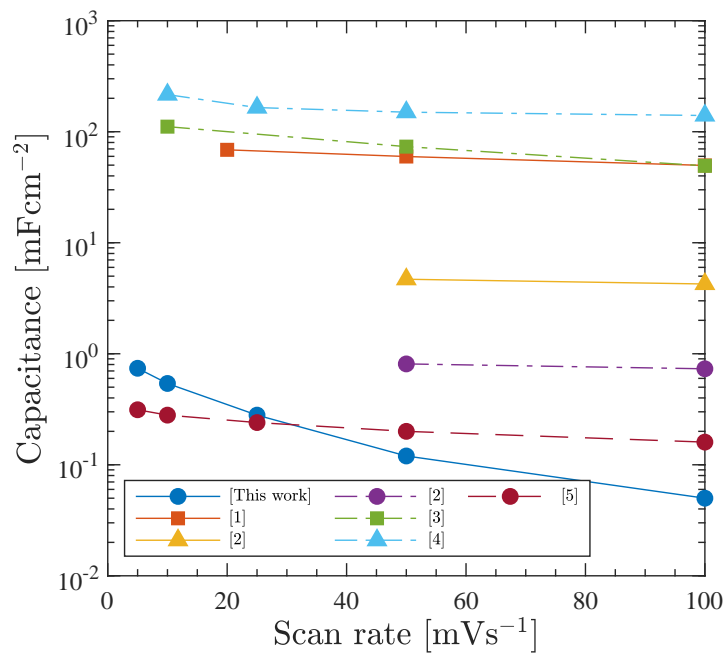


Figure 6-1: The current place of this work and future outlooks for further development.

Bibliography

- [1] Y. Neuvoo and S. Ylönen. Bit Bang: Rays to the future. Technical report, Helsinki University of Technology, 2010.
- [2] Katsuaki Suganuma. *Printing Technology, Conducting Materials for Printed Electronics*, pages 23–48, 49–74. Springer New York, New York, NY, 2014.
- [3] Xin Li, Taoli Gu, and Bingqing Wei. Dynamic and galvanic stability of stretchable supercapacitors. *Nano letters*, 12(12):6366–6371, 2012.
- [4] Xiran Li, Hongpeng Li, Xiangqian Fan, Xinlei Shi, and Jiajie Liang. 3d-printed stretchable micro-supercapacitor with remarkable areal performance. *Advanced Energy Materials*, 10(14):1903794.
- [5] Anne Håkansson. Portal of research methods and methodologies for research projects and degree projects. pages 67–73, Las Vegas USA, 2013. KTH, Skolan för informations- och kommunikationsteknik (ICT), Programvaruteknik och Datorsystem, SCS, CSREA Press U.S.A.
- [6] Khasha Ghaffarzadeh and James Hayward. Stretchable and conformable electronics: Heading toward market reality. *Information Display*, 33(6):28–31, 2017.
- [7] J Chang, Tong Ge, and E Sanchez-Sinencio. Challenges of printed electronics on flexible substrates. In *2012 IEEE 55th International Midwest Symposium on Circuits and Systems (MWSCAS)*, pages 582–585. IEEE, 2012.
- [8] *Flexible Electronics Materials and Applications*. Electronic Materials: Science Technology, 11. 1st ed. 2009.. edition, 2009.
- [9] Yunlei Zhou, Chaoshan Zhao, Jiachen Wang, Yanzhen Li, Chenxin Li, Hangyu Zhu, Shuxuan Feng, Shitai Cao, and Desheng Kong. Stretchable high permittivity nanocomposites for epidermal alternating current electroluminescent displays. *ACS Materials Letters*, 2019.
- [10] Yuhao Liu, Matt Pharr, and Giovanni Antonio Salvatore. Lab-on-skin: A review of flexible and stretchable electronics for wearable health monitoring. *ACS Nano*, 11(10):9614–9635, 2017. PMID: 28901746.

- [11] Anindya Nag. *Printed Flexible Sensors Fabrication, Characterization and Implementation*. Smart Sensors, Measurement and Instrumentation, 33. 1st ed. 2019.. edition, 2019.
- [12] Szymon Sollami Delekta, Karin H. Adolfsson, Nejla Benyahia Erdal, Minna Hakkarainen, Mikael Stling, and Jiantong Li. Fully inkjet printed ultrathin microsupercapacitors based on graphene electrodes and a nano-graphene oxide electrolyte. *Nanoscale*, 11(21):10172–10177, 2019.
- [13] Jiantong Li, Szymon Sollami Delekta, Panpan Zhang, Sheng Yang, Martin R. Lohe, Xiaodong Zhuang, Xinliang Feng, and Mikael Östling. Scalable fabrication and integration of graphene microsupercapacitors through full inkjet printing. *ACS Nano*, 11(8):8249–8256, 2017. PMID: 28682595.
- [14] Alejandro Espera, John Dizon, Qiyi Chen, and Rigoberto Advincula. 3d-printing and advanced manufacturing for electronics. *Progress in Additive Manufacturing*, 4(3):245–267.
- [15] Francois Beguin. *Supercapacitors: Materials, Systems, and Applications*. New Materials for Sustainable Energy and Development Ser. 1st ed. edition, 2013.
- [16] Ye Wang, Yumeng Shi, Cheng Xi Zhao, Jen It Wong, Xiao Wei Sun, and Hui Ying Yang. Printed all-solid flexible microsupercapacitors: towards the general route for high energy storage devices. *Nanotechnology*, 25(9):094010, 2014.
- [17] Ke Sun, Teng-Sing Wei, Bok Yeop Ahn, Jung Yoon Seo, Shen J. Dillon, and Jennifer A. Lewis. 3d printing of interdigitated li-ion microbattery architectures. *Advanced Materials*, 25(33):4539–4543, 2013.
- [18] Milad Areir, Yanmeng Xu, Ruirong Zhang, David Harrison, John Fyson, and Eujin Pei. A study of 3d printed active carbon electrode for the manufacture of electric double-layer capacitors. *Journal of Manufacturing Processes*, 25:351–356, 2017.
- [19] Wei Yu, Han Zhou, Ben Q Li, and Shuijiang Ding. 3d printing of carbon nanotubes-based microsupercapacitors. *ACS applied materials interfaces*, 9(5):4597–4604, 2017.

- [20] Milad Areir, Yanmeng Xu, David Harrison, and John Fyson. A study of 3d printed flexible supercapacitors onto silicone rubber substrates. *Journal of Materials Science: Materials in Electronics*, 28(23):18254–18261, 2017.
- [21] 3d printing of interdigitated electrode for all-solid-state microsupercapacitors. *Journal of Micromechanics and Microengineering*, 28(10):105014, 2018.
- [22] Xiawei Yun, Bingchuan Lu, Zhiyuan Xiong, Bo Jia, Bo Tang, Henan Mao, Ting Zhang, and Xiaogong Wang. Direct 3d printing of a graphene oxide hydrogel for fabrication of a high areal specific capacitance microsupercapacitor. *RSC Advances*, 9(50):29384–29395, 2019.
- [23] Yi-Zhou Zhang, Yang Wang, Tao Cheng, Lan-Qian Yao, Xiangchun Li, Wen-Yong Lai, and Wei Huang. Printed supercapacitors: materials, printing and applications. 48(12):3229–3264, 2019.
- [24] La Li, Zheng Lou, Di Chen, Kai Jiang, Wei Han, and Guozhen Shen. Recent advances in flexible/stretchable supercapacitors for wearable electronics. *Small*, 14(43):n/a–n/a, 2018.
- [25] William D. Callister. *Materials science and engineering*. Wiley, Hoboken, NJ, 8th ed.. edition, 2011.
- [26] A.M. Nardes. On the conductivity of pedot:pss thin films. 2007.
- [27] Xiaowei Yu, Bikram K. Mahajan, Wan Shou, and Heng Pan. Materials, mechanics, and patterning techniques for elastomer-based stretchable conductors. *Micromachines*, 8(1):7, 2016.
- [28] Laure V. Kayser and Darren J. Lipomi. Stretchable conductive polymers and composites based on pedot and pedot:pss. *Advanced Materials*, 31(10):1806133, 2019.
- [29] Xi Fan, Wanyi Nie, Hsinhan Tsai, Naixiang Wang, Huihui Huang, Yajun Cheng, Rongjiang Wen, Liuji Ma, Feng Yan, and Yonggao Xia. Pedot:pss for flexible and stretchable electronics: Modifications, strategies, and applications. *Advanced Science*, 6(19):n/a–n/a, 2019.
- [30] Chen Zhao, Caiyun Wang, Zhilian Yue, Kewei Shu, and Gordon G Wallace. Intrinsically stretchable supercapacitors composed of polypyrrole electrodes and highly stretchable gel electrolyte. *ACS applied materials interfaces*, 5(18):9008–9014, 2013.

- [31] Yue Wang, Chenxin Zhu, Raphael Pfattner, Hongping Yan, Lihua Jin, Shucheng Chen, Francisco Molina-Lopez, Franziska Lissel, Jia Liu, Noelle I Rabiah, Zheng Chen, Jong Won Chung, Christian Linder, Michael F Toney, Boris Murmann, and Zhenan Bao. A highly stretchable, transparent, and conductive polymer. *Science Advances*, 3(3), 2017.
- [32] Zhisheng Lv, Yuxin Tang, Zhiqiang Zhu, Jiaqi Wei, Wenlong Li, Huarong Xia, Ying Jiang, Zhiyuan Liu, Yifei Luo, Xiang Ge, Yanyan Zhang, Renheng Wang, Wei Zhang, Xian Jun Loh, and Xiaodong Chen. Honeycomb-lantern-inspired 3d stretchable supercapacitors with enhanced specific areal capacitance. *Advanced Materials*, 30(50):n/a–n/a, 2018.
- [33] Juan Pu, Xiaohong Wang, Renxiao Xu, and Kyriakos Komvopoulos. Highly stretchable microsupercapacitor arrays with honeycomb structures for integrated wearable electronic systems. *ACS nano*, 10(10):9306–9315, 2016.
- [34] Jianfeng Zang, Changyong Cao, Yaying Feng, Jie Liu, and Xuanhe Zhao. Stretchable and high-performance supercapacitors with crumpled graphene papers. *Scientific Reports*, 4(1), 2014.
- [35] Yihao Zhou, Changyong Cao, Yunteng Cao, Qiwei Han, Charles B. Parker, and Jeffrey T. Glass. Robust and high-performance electrodes via crumpled au-cnt forests for stretchable supercapacitors. *Matter*, 2020.
- [36] Cunjiang Yu, Charan Masarapu, Jiepeng Rong, Bingqing Wei, and Hanqing Jiang. Stretchable supercapacitors based on buckled single-walled carbon-nanotube macrofilms. *Advanced Materials*, 21(47):4793–4797, 2009.
- [37] Zhiqiang Niu, Haibo Dong, Bowen Zhu, Jinzhu Li, Huey Hoon Hng, Weiya Zhou, Xiaodong Chen, and Sishen Xie. Highly stretchable, integrated supercapacitors based on single-walled carbon nanotube films with continuous reticulate architecture. *Advanced Materials*, 25(7):1058–1064, 2013.
- [38] Lu-Yu Zhou, Jian-Zhong Fu, Qing Gao, Peng Zhao, and Yong He. All-printed flexible and stretchable electronics with pressing or freezing activatable liquid-metal–silicone inks. *Advanced Functional Materials*, 30(3), 2020.
- [39] Sangbaek Park, Hyub Lee, Young-Jin Kim, and Pooi See Lee. Fully laser-patterned stretchable microsupercapacitors integrated with soft electronic circuit components. *NPG Asia Materials*, 10(10):959–969, 2018.

- [40] Zhibin Yang, Jue Deng, Xuli Chen, Jing Ren, and Huisheng Peng. A highly stretchable, fiber-shaped supercapacitor. *Angewandte Chemie International Edition*, 52(50):13453–13457, 2013.
- [41] Anton V. Volkov, Kosala Wijeratne, Evangelia Mitraka, Ujwala Ail, Dan Zhao, Klas Tybrandt, Jens Wenzel Andreasen, Magnus Berggren, Xavier Crispin, and Igor V. Zozoulenko. Understanding the capacitance of pe-dot:pss.(report). *Advanced Functional Materials*, 27(28):n/a, 2017.
- [42] ViscoTec Pumpen Dosiertechnik GmbH. Print Heads For Viscous Fluids In 3D Printing. <https://www.viscotec.de/media/broschueren-druckkoepfe-3-d-viscotec-en-1017-web2.pdf>. [Online; accessed 15 March 2020].
- [43] FELIXPrinters. User Manual FELIX Pro 2. https://www.felixprinters.com/shop/downloads_felixprinters, 2018. [Online; accessed 10 March 2020].

Appendix

Table 6.1: Capacitance values of fabricated devices.

Scan rate [mV s ⁻¹]	5	10	25	50	100
Capacitance [μF cm ⁻²]					
1L_EL1_1	270.3	198.0	114.4	57.19	24.16
1L_EL1_2	309.3	222.2	120.6	56.58	22.86
2L_EL1_1	443.6	298.4	120.3	48.8	20.3
2L_EL1_2	424.6	280.5	108.9	45.0	19.4
4L_EL1_1	3185	1971.4	1059.1	584.6	252.3
2L_EL2_1	182.4	72.9	21.4	9.4	4.3
2L_EL2_1	741.3	428.8	170.1	65.2	24.9
2L_EL3_1	693.8	507.0	257.0	111.9	44.2
2L_EL3_2	786.3	582.6	313.0	144.7	59.3

